The PN_t-Methodology: a top-down network modelling approach to estimate dose- and time-dependent cell responses to complex multifactorial environments

Laura Baumgartner[1*], Miguel Ángel González Ballester[1,2], Jérôme Noailly[1]

[1]Biomechanics and Mechanobiology, BCN MedTech, Information and Communication Technologies, Universitat Pompeu Fabra, Barcelona, Spain

[2]ICREA, Barcelona, Spain

*** Correspondence:** Laura Baumgartner, laura.baumgartner@upf.edu

Keywords: systems biology, multicellular level, parallel networks, multifactorial environment, time sensitivity, dose sensitivity

Abstract

Current methodologies to estimate cell responses usually focus on bottom-up intracellular network modeling, accompanied by limitations regarding the network topology and regarding the consideration of transient changes in cell responses due to chronic, dose-dependent stimulus exposure. Here we present a novel high-level top-down network modelling approach to simulate dose- and time-dependent cell responses within heterogeneous multifactorial, multicellular environments. Through the representation of cell activities as time-dependent parallel networks (PN_t), the PN_t-Methodology provides relative, interrelated cell responses for heterogeneous stimulus environments. The methodology is based on a systematic use of experimental findings, both data- and knowledge-based. Applied to intervertebral disc multicellular systems,

the PN_t-Methodology allows for the first time to obtain qualitatively validated cell responses for daily human moving activities and exposure to microgravity. The PN_t-Methodology is not tissue specific per-se and is designed to be easily scalable. Eventually, it provides a one-of-a-kind network modeling approach to approximate complex multicellular systems.

Introduction

Highly multifactorial disorders are difficult to apprehend, since an approximation of cell responses to heterogeneous sets of stimuli (i.e. varying stimulus combinations in close cellular neighborhood) is challenging. Multifactorial disorders usually evolve slowly and silently and are believed to be strongly influenced by environmental factors. Hence, a better understanding of the effect of such factors on cell responses is cornerstone to tackle slowly developing multifactorial diseases. Advances in experimental and *in silico* research importantly enhanced our understanding of intracellular regulations and cell responses to environmental cues, leading to extensive databases on signaling pathways and protein-protein interactions (Baumgartner et al., 2021) and modeling approaches to simulate complex cell dynamics. Accordingly, numerical methods usually focus on bottom-up descriptions using logic modeling such as Boolean or fuzzy-logic formalisms and ordinary differential equation (ODE) approaches (Aldridge et al., 2009; Khurana et al., 2021; Krumsiek et al., 2010; Mendoza and Xenarios, 2006; Mitsos et al., 2012; Morris et al., 2010; Orton et al., 2005; Yue et al., 2006), to define graph-based (or network) models based on knowledge. However, it is challenging to define directionality for such models and changes in network topology might importantly alter final network responses. Moreover, an integration of the growing experimental knowledge into network models is not straightforward and requires often a reduction of

network topology and network fitting, to define proper trade-offs between knowledge and data incorporation (Khurana et al., 2021; Segarra-Queralt et al., 2022). Eventually, graph-based models usually lead to steady-state nodal activations, often neglecting the effect of both the time and the dose of a stimulus.

To this end, we propose a new methodology to approximate complex heterogeneous dose-and time-dependent multicellular systems by introducing a top-down network modelling approach. We present this methodology as the PN_t-Methodology. Thereby, the cell per-se is considered as a “black box” and crucial cell activities (CA) are estimated by linking them to their multifactorial environment based on experimental knowledge. The different CA that are simultaneously regulated by the multifactorial environment are conceptualized as potentially time-dependent (subscript t) parallel networks (PN). The PN_t-Methodology consists of a set of methods to (i) translate biological findings into parameters suitable for systems biology approaches (Baumgartner et al., 2021a, 2021b), (ii) an approach to estimate the effect dose-and time dependency over long time-periods on a CA, and (iii) a core element, an ODE-based equation, to link the effect of multifactorial stimulus environments on CA of multicellular systems.

The PN_t-Methodology was developed to investigate the initiations of intervertebral disc (IVD) degeneration, an illustrative case for a multifactorial disorder. Thereby, the tissue in the center of the IVD, the Nucleus Pulposus (NP) was tackled. We could demonstrate that the PN_t-Methodology provides a novel solution for forward estimations of the CA of cells within multicellular systems exposed to multifactorial heterogenous stimulus environments, including time-dependent responses over long time periods.

Results

Determination of the system of interest. A stimulus environment usually consists of local stimuli and of stimuli coming from a distant source, introduced here as “external” stimuli. These are nutrition-related or mechanical stimuli. It is hypothesized that alterations in CA are not spontaneous processes, but initially caused by alterations of external stimuli, which subsequently affect the cell homeostasis and local stimulus expressions.

Cell responses can be reflected as profiles of *n* crucial CA, regulated by a multifactorial environment of *m* stimuli. Thereby, a stimulus can either activate, or inhibit or dose- and/or time-dependently alter a CA. Time- and dose-dependent stimuli can be either activating or inhibiting depending on the dose and/or the duration of the stimulus. Moreover, *p* different cell states (CS) might co-exist within a representative volume of cells due to local expressions of key stimuli, e.g. locally synthesized proinflammatory cytokines (Figure 1, top) that generate a heterogeneous cell environment.

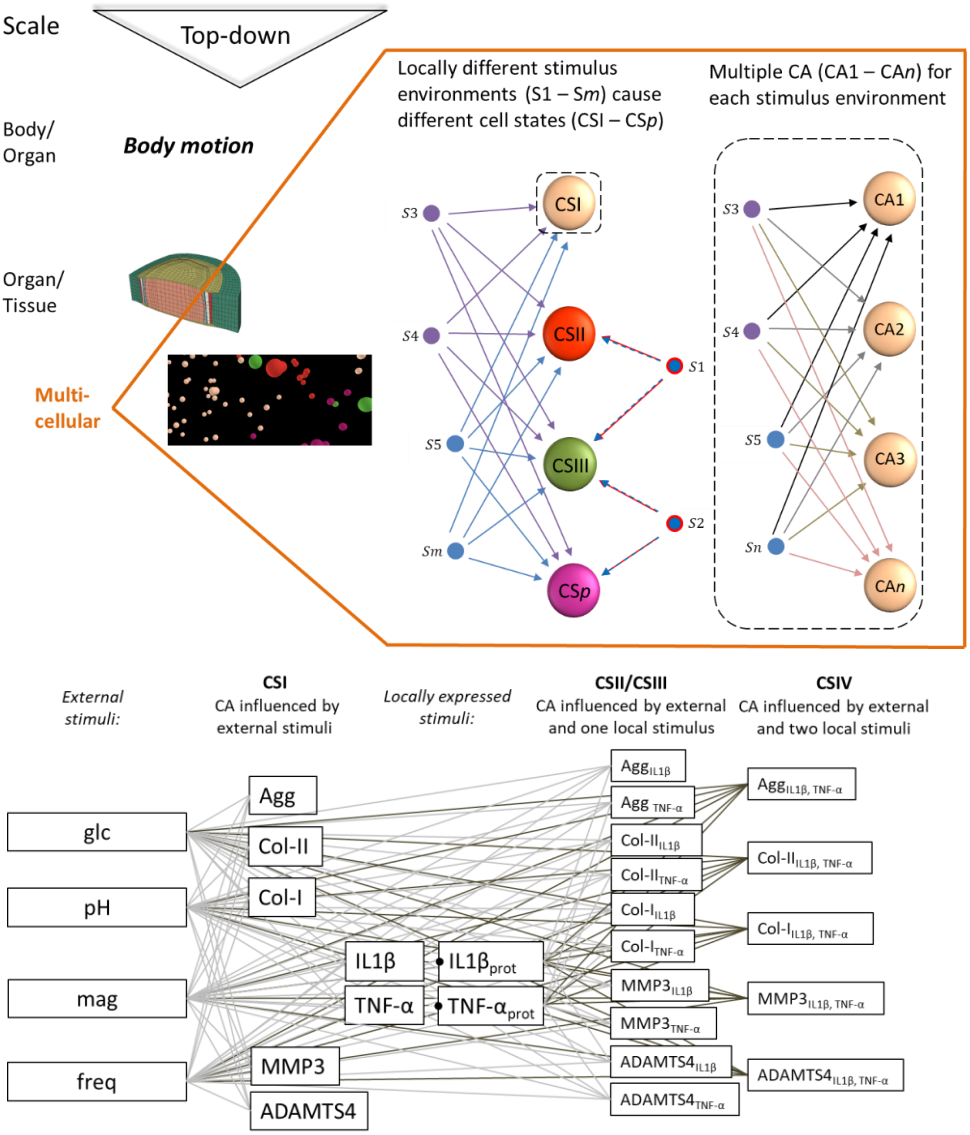

Figure 1: Top: the PN_t-Methodology tackles the multicellular level. Schematic visualization of a complex, multifactorial, multicellular environment, consisting of *m* stimuli, *p* cell states (CS) and *n* cell activities (CA). Individual stimulus-CA interactions (arrows) might have an activating (blue; *S1*, *S2*, *S5*, *Sm*, *Sn*), inhibiting (red; *S1*, *S2*) or a time-dependent (purple; *S3*, *S4*) effect on a CA. Below: PN_t-Methodology applied to approximate NP cell behavior. The system of interest consists of four external key stimuli (glc, pH, mag, freq) and the CA enclose the mRNA expressions of tissue proteins (Agg, Col-I, Col-II) and proteases (MMP3, ADAMTS4). Different cell states (CSI-IV) were induced by the presence of the locally expressed proinflammatory cytokines TNF-α and IL1β.

Based on this concept, tissue-specific systems of interest were determined (Figure 1, below). Key relevant stimuli in NP cell regulations were identified based on literature. External stimuli were the nutrient-related stimuli glucose (glc) and pH and the mechanical parameters magnitude (mag) and frequency (freq) (Chan et al., 2011; Gilbert et al., 2016; Kerr et al., 2017; Rinkler et al., 2010; Saggese et al., 2018). The locally expressed stimuli were chosen to be proinflammatory cytokines, since these were found to be critical factors in IVD degeneration (Gorth et al., 2015; Johnson et al., 2015). Thereby, interleukin 1β (IL1β) and the tumor necrosis factor α (TNF-α) were classically related to initiations of this disorder (Johnson et al., 2015). Considering two local stimuli, a NP cell can obtain one out of four different proinflammatory CS: non-inflamed or inflamed for either IL1β, TNF-α or for both, IL1β&TNF-α. Estimated cell responses were the mRNA expressions of the NP tissue components Aggrecan (Agg) and Collagen Types I and II (Col-I, Col-II) (Baumgartner et al., 2021), and proteases MMP3 and ADAMTS4 from the matrix metalloprotease (MMP) and the "a disintegrin and metalloproteinase with thrombospondin motifs" (ADAMTS) families, since those CA were deemed to be key relevant in IVD degeneration (Baumgartner et al., 2021; Kerr et al., 2017; Molinos et al., 2015).

Feeding the system of interest with evidence-based parameters and relate it to relevant PN-systems. PN-systems are subsystems of the system of interest and must be defined prior to calculations. A PN-system contains all the CA that are required to have an interrelated expression. In the current system of interest of the NP, an interrelated expression of tissue proteins and proteases of each CS is desired. In contrast, the prediction of local stimuli (proinflammatory cytokines) determines CSII, III and IV (Figure 1, below) and require separate PN-systems, as these local stimuli serve as input parameters for an inflammation submodel that semi-quantitatively estimates the

concentration of the local stimulus protein concentration (Baumgartner et al., 2021b), based on external stimulus concentrations. A PN-system consists of directed parallel networks. A parallel network considers the stimuli that surround a cell and regulate a specific CA (see Methods, Figure 7). For example, the parallel network to determine Agg of non-inflamed cells (CSI, Figure 1) consists of the stimuli glc, pH, mag and freq and the CA Agg mRNA expression.

External stimulus doses cover physiologically relevant ranges for a given tissue. For the NP, this includes glc concentrations of 0 mM – 5 mM, a pH 6.5-7.4, load mag of 0.1 MPa – 3.5 MPa and freq of 0 Hz – 40 Hz (Figure 2, A).

Connections between a stimulus and a CA are defined as S-CA relationships and are determined by the sensitivity of a CA to a stimulus type and the stimulus dose. A stimulus dose refers to biochemical stimulus concentrations or to load intensities. Parameters that estimate the effect of a stimulus type and dose on a CA are obtained from experimental findings as previously explained (Baumgartner et al., 2021a, 2021b). In short: the sensitivity of a CA to a stimulus (subscript S) dose is reflected as x_S^{CA}. x_S^{CA} can obtain values between 0 and 1 and is optimally obtained by a continuous sigmoidal function that relates each physiologically relevant stimulus concentration to a value for x_S^{CA} (Figure 2, B) (Baumgartner et al., 2021a, 2021b). Thereby, 0 reflects a minimal and 1 a maximal activity of a CA for a given stimulus concentration. The effect of the stimulus type was defined through a weighting factor (θ_S^{CA}) (Figure 2, B). Weighting factors can obtain values of $0.01 \leq \theta_S^{CA} \leq 1$ and are determined based on the maximal x-fold change in mRNA expression caused by differences in stimulus concentrations (Baumgartner et al., 2021b). Thereby, the lowest weighting factor of 0.01 was assigned to non-significant S-CA relationships (Figure 2, A, dashed lines).

For the system of interest of NP cells, specific weighting factors of the S-CA relationships of the stimuli glc, pH, TNF-α and IL1β were previously presented (Baumgartner et al., 2021b) and newly obtained for the stimuli mag and freq (Methods).

The quality of S-CA relationships is either activating, inhibiting or dose-and/or time-dependent (blue, red or purple, respectively) (Figure 2, A).

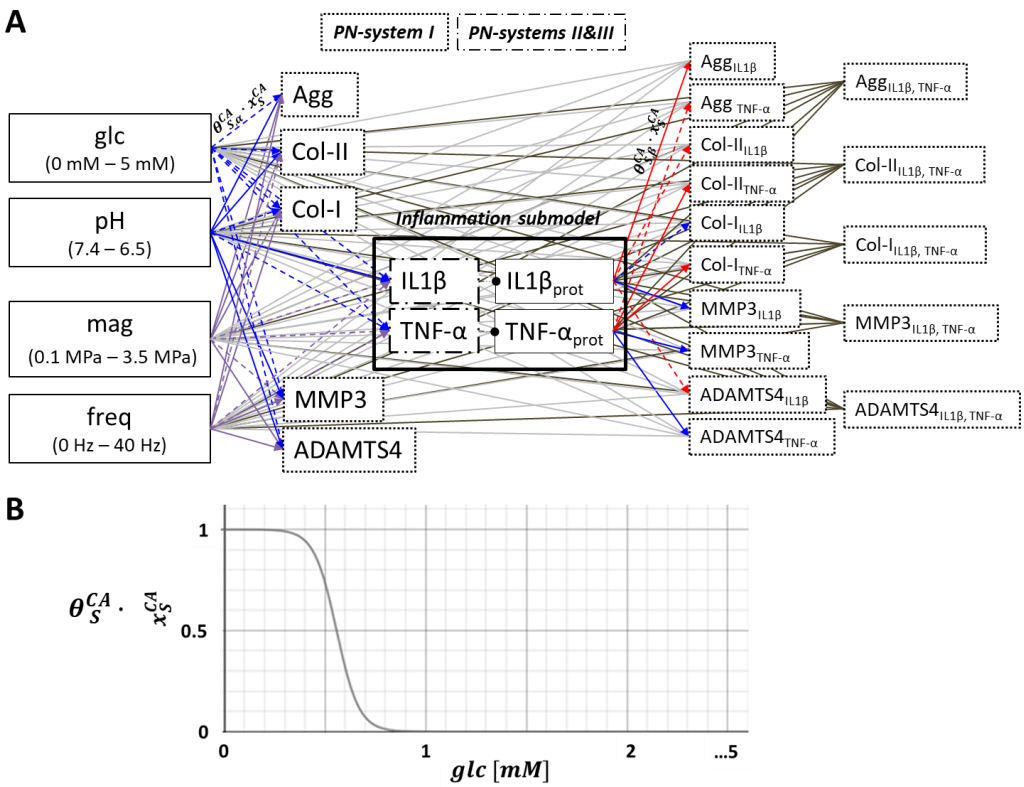

Figure 2: A: System of interest, subdivided into relevant PN-systems. Arrows reflect the nature of individual stimulus-cell activity (S-CA) relationships, being either activating (blue), inhibiting (red) or dose- and time-dependent (purple). Non-significant S-CA relationships are marked with dashed lines. The proinflammatory environment is estimated by an inflammation submodel (Baumgartner et al., 2021b). B: S-CA relationships are determined by a weighting factor (θ_S^{CA}) and a normalized sensitivity of a CA to a stimulus concentration (x_S^{CA}). Example: glucose (glc)-MMP3 relationship.

Stimuli can either be steadily present under relatively constant concentrations, or strongly fluctuating. Within the NP, nutrients were assumed to be generally present. Therefore, current nutrient concentrations were used to determine a basal level for each

CA. They were considered to be always (to a smaller or bigger extent) activating (Baumgartner et al., 2021b). Proinflammatory cytokines were integrated as constantly activating or inhibiting, depending on the considered CA (Figure 2, A). Assumptions are based on experimental data from cell cultures (Baumgartner et al., 2021b). In contrast, mechanical load parameters, i.e., mag and freq, depended on the physical behavior of a person. The effect of the mechanical load on a CA depended on the stimulus dose and on the exposure time (Chan et al., 2011), and it could be either anabolic or catabolic (see Results, section "Approximation of stimuli with dose-dependent anabolic or catabolic impact.").

Calculating PN-systems with the PN-equation. The PN-equation is an ODE-based approach to resolve PN-systems (Eq. 1).

$$\frac{d\omega_{CA,CS}}{dt} = \left(\left(\frac{1+\sum\theta_{\alpha}}{\sum\theta_{\alpha}}\right)\left(\frac{\sum\theta_{S,\alpha}^{CA}x_{S,\alpha}^{CA}}{1+\sum\theta_{S,\alpha}^{CA}x_{S,\alpha}^{CA}}\right)\right)\cdot\left(1-\left(\left(\frac{\sum\theta_{S,\beta}^{CA}}{\sum\theta_{S,\alpha}^{CA}+\sum\theta_{S,\beta}^{CA}}\right)\left(\left(\frac{1+\sum\theta_{\beta}^{CA}}{\sum\theta_{\beta}^{CA}}\right)\left(\frac{\sum\theta_{S,\beta}^{CA}x_{S,\beta}^{CA}}{1+\sum\theta_{S,\beta}^{CA}x_{S,\beta}^{CA}}\right)\right)\right)\right) \quad (1)$$

The PN-equation was developed based on a well-established, graph-based analytical methodology to approximate single network dynamics (Mendoza and Xenarios, 2006) (Methods). It determines a time-dependent overall activation of a CA of each CS ($\frac{d\omega_{CA,CS}}{dt}$) and is built of an activating and an inhibiting term (subscript α and β, respectively). Thereby, the activating and inhibiting parts of the equation combined two and three fractional terms, respectively. The first fractional term of the activating part determines the maximal activation by considering all activating weighting factors (θ_{α}) within the PN-system. The second fraction determines the activation of the tackled CA by integrating all its activating S-CA relationships ($\theta_{S,\alpha}^{CA}x_{S,\alpha}^{CA}$). The inhibition is determined relative to the activation of a particular CA. The first fraction determines the

relative weight of the inhibition, the second fraction the maximal inhibiting weight of a CA, independently of the CS (θ_{β}^{CA}) and the third fraction reflects the actual inhibition of the tackled CA ($\theta_{S,\beta}^{CA} x_{S,\beta}^{CA}$). Both, the activating and inhibiting parts are explained in detail in Methods.

To enable the contribution of a stimulus to either the activating or the inhibiting part depending on the exposure time, the weighting factor, θ, of this stimulus must be listed in both the activating and inhibiting parts of the PN-equation. The weighting factor within the term, where the stimulus is initially not active is determined as "completive weighting factor" (indexed with δ) and can be understood as placeholder within the PN-equation. Completive weighting factors have the same value as their counterparts. Hence, if the weighting factor that describes the impact of mag on Agg equals 0.3484 ($\theta_{mag}^{Agg} = 0.3484$) (see Table 3, Methods) the corresponding, completive weighting factor, i.e. ($\theta_{\delta,mag}^{Agg}$) has the same value. An example of a complete PN-equation for the PN-system I is shown in Methods, Figure 10, Eq. 6 and the general approach to obtain PN-equations for PN-systems II and III in Eq. 7.

The results of the PN-equation, i.e., overall CA ($\frac{d\omega_{CA,CS}}{dt}$), are calculated as dimensionless PN-activities. The higher a PN-activity for a certain CA, the higher is the relative upregulation of that specific CA. PN-activities have a resolution of 4 decimals (Baumgartner et al., 2021b) and can take values between 0 and 1. The specific range over which an individual CA can vary is determined by the weighting factors of that CA. Hence, the more impact a CA has within the PN-system, the wider is the range of values it can obtain. As a result, PN-activities reflect the relative activations of different CA within the same PN-system. If the user wants to know the maximal PN-activity for

a CA, $x_{S,\alpha}^{CA}$ must be set to 1 and the inhibiting portion of the PN-equation must be 0. PN-activities continuously determine the actual CA at each user-defined timestep. To compare the CA associated with different physical activities after a given period of time, an accumulation of PN-activities (acc. PN-activity) can be calculated. This holds true also to obtain cell responses after a sequence of different physical activities (e.g. cell responses after an average day on Earth, last section of Results, Figure 5).

Approximation of stimuli with dose-dependent anabolic or catabolic impact. To determine the anabolic and catabolic effects of a stimulus depending on its dose, logistic functions were used to determine x_S^{CA}, similar to nutrition-related stimuli (Figure 2, B), but the range was extended to [-1;1], so that $-1 \leq x_S^{CA} \leq 1$. Thereby, $0 < x_S^{CA} \leq 1$ reflects an activating effect of the stimulus and is integrated within the active portion of the PN-equation ($x_{S,\alpha}^{CA}$). In contrast, $0 > x_S^{CA} \geq -1$ reflects an inhibiting effect on $\omega_{CA,CS}$ and is integrated within the inhibiting portion ($x_{S,\beta}^{CA}$) of the PN-equation. Note that only the absolute values of x_S^{CA} are fed into the PN-equation, as it only accepts positive values for x_S^{CA} bound between 0 and 1 (see Methods). Hence, the sign provided by the logistic function indicates the part of the PN-equation in which the value of x_S^{CA} should take a role. $x_S^{CA} = 0$ reflects the transition from activating to inhibiting and is determined as α-β-threshold.

Relevant, stimulus ranges and specific logistic functions for the NP were determined based on *in vivo* studies (Methods) and are referred to as generic functions (X_S). Thereby, low mag and freq were assumed to be anabolic and become catabolic under rising load intensities. Consequently, in the anabolic range of the load parameter values, CA is activated for tissue proteins and inhibited for proteases, whereas in the catabolic range CA is inhibited for tissue proteins and activated for proteases. Hence, two generic

functions X_S were determined for both mag and freq and were mirrored with respect to the α-β-threshold (Figure 3 A, B). Generic functions evolving with rising stimulus intensities, from activating to inhibiting were labelled with superscripts A;I ($X_S^{A;I}$) and those evolving from inhibiting to activating were labelled with superscripts I;A ($X_S^{I;A}$). Though, related to the NP, Agg and Col-II mRNA expressions were associated to the functions $X_{Mag}^{A;I}$ and $X_{Freq}^{A;I}$, respectively, whilst any other mRNA expression were associated to $X_{Mag}^{I;A}$and $X_{Freq}^{I;A}$. The generic function for mag was exemplarily shown in Figure 3, A ,B.

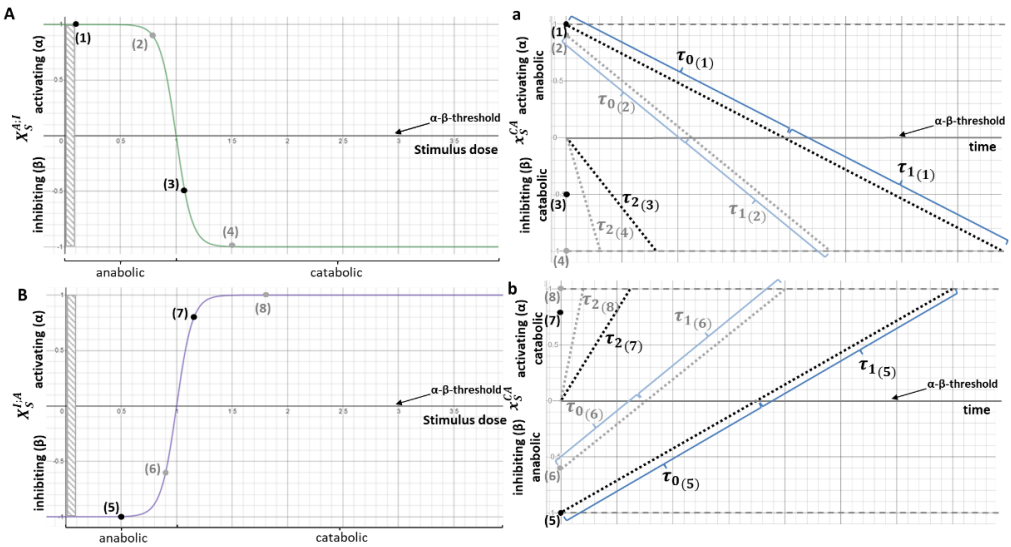

Figure 3: Illustration of mirrored generic functions ($\boldsymbol{X_S^{A;I}}$,$\boldsymbol{X_S^{I;A}}$) evolving from activating to inhibiting (A;I) (A) and from inhibiting to activating (I;A) (B) under rising stimulus intensities. a, b illustrate the time dependency ($\boldsymbol{\tau}$) that finally determines $\boldsymbol{x_S^{CA}}$. The influence of the stimulus dose on the time-sensitivity was schematically sketched for eight randomly chosen stimulus intensities ((1)-(8)); four on each mirrored generic function (A and B). Hence, the anabolic effect of the most anabolic stimulus dose ((1), A) remains over longer time periods ((1) a) than a less anabolic stimulus (e.g. (2) A, a). Time dependencies reflect a loss of activation due to a stimulus exposure over time ($\boldsymbol{\tau_0}$) and a corresponding active inhibition after passing the α-β-threshold ($\boldsymbol{\tau_1}$). For initially catabolic stimulus intensities, a latency time before developing a maximal negative impact on a CA was considered ($\boldsymbol{\tau_2}$) (see next subsection regarding the determination and integration of time-sensitivity). Maximal $\boldsymbol{x_S^{CA}}$ are 1 and -1, respectively.

Determination and integration of time-sensitivity. Values provided by the generic functions were coupled to a time sensitivity term (τ) to eventually obtain x_S^{CA}. τ depends on three variables; the initial stimulus dose (obtained through X_S), a CA-specific time sensitivity (γ_S^{CA}) and the stimulus exposure time (t). The time effect includes (i) a loss of anabolic stimulus over time, and (ii) a time delay in the development of a catabolic response to a catabolic stimulus (Table 1).

Table 1: mathematical description of the time sensitivity term ($\boldsymbol{\tau}$) and the sensitivity of CA to a stimulus dose ($\boldsymbol{x_S^{CA}}$). Note that integration into the PN-equation requires positive values. Hence, absolute values were used for the terms known to be negative. A;I: generic functions that evolve from activating to inhibiting. I;A: generic functions that evolve from inhibiting to activating. $\boldsymbol{\tau}$ are schematically plotted in Figure 3, a (A;I) and b (I;A), respectively.

	Range	**Time-sensitivity term (τ)**	**Time-dependent sensitivity of a CA to a stimulus dose**
A;I	anabolic	$\tau_0 = (1 - X_S^{\mathrm{A;I}}) \cdot \gamma_{S,ana}^{CA} \cdot t$	$x_S^{CA} = X_S^{\mathrm{A;I}} - \tau_0$
	catabolic	$\tau_1 = (1 - X_S^{\mathrm{A;I}}) \cdot \gamma_{S,ana}^{CA} \cdot (t - t_{\tau_0})$	$x_S^{CA} = \lvert 0 - \tau_1 \rvert$
		$\tau_2 = \lvert X_S^{\mathrm{A;I}} \rvert \cdot \gamma_{S,cata}^{CA} \cdot (t + 1)$	$x_S^{CA} = \lvert 0 - \tau_2 \rvert$
I;A	anabolic	$\tau_0 = (\lvert (-1) + \lvert X_S^{\mathrm{I;A}} \rvert \rvert) \cdot \gamma_{S,ana}^{CA} \cdot t$	$x_S^{CA} = \lvert X_S^{\mathrm{I;A}} + \tau_0 \rvert$
	catabolic	$\tau_1 = (\lvert (-1) + \lvert X_S^{\mathrm{I;A}} \rvert \rvert) \cdot \gamma_{S,ana}^{CA} \cdot (t - t_{\tau_0})$	$x_S^{CA} = 0 + \tau_1$
		$\tau_2 = X_S^{\mathrm{I;A}} \cdot \gamma_{S,cata}^{CA} \cdot (t + 1)$	$x_S^{CA} = 0 + \tau_2$

The formulation of τ varies depending on the initial stimulus dose. τ_0 defines the loss of the effect of an initially anabolic stimulus over time. After passing the individual α-β-threshold τ_1 is activated. τ_1 has the same mathematical description as τ_0, but considers as a time origin the individual time point (t_{τ_0}), when the α-β-threshold was crossed (Figure 3, a, b). τ_2 describes the time delay for a catabolic stimulus to reach its whole catabolic potential, which affects already the first hour of stimulus exposure. The effect of time sensitivity is applied until a maximal activating (1) or inhibiting ($|-1|$) impact of a stimulus is reached (Figure 3, a, b).

The velocity at which the anabolic effect of a stimulus decreases, or at which the catabolic effect increases depends on the stimulus dose. It was either obtained by the absolute difference between 1 and $X_S^{A;I}$ and $X_S^{I;A}$ and -1, respectively (τ_0,τ_1) or by the (absolute) value of X_S (τ_2) (Figure 4, Table 1).

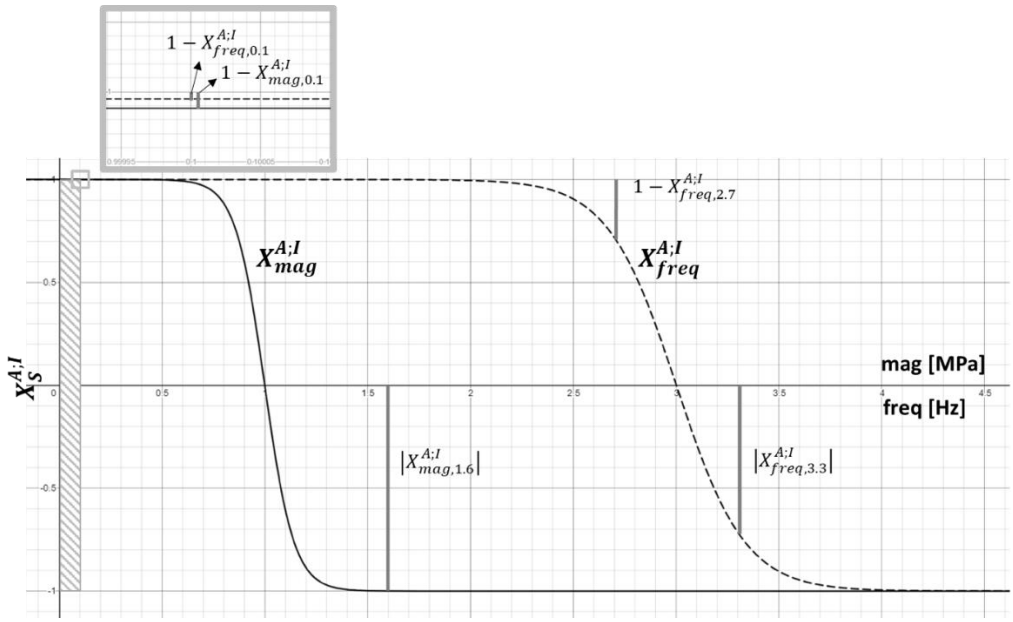

Figure 4: determination of the influence of a stimulus dose on the velocity (e.g. for freq = 2.7 Hz within the anabolic range, velocity is: $\frac{\partial \tau_0}{\partial t} = (\mathbf{1} - \boldsymbol{X}^{\mathbf{A;I}}_{\boldsymbol{freq}\ \mathbf{2.7}}) \cdot \boldsymbol{\gamma}^{\boldsymbol{CA}}_{\boldsymbol{freq,ana}}$) at which the anabolic effect of the stimulus gets lost or at which the catabolic effect reaches its whole potential. Example for $\boldsymbol{X}^{\boldsymbol{A;I}}_{\boldsymbol{S}}$ functions of mag and freq. Illustrations for the stimulus intensities at 0.1 MPa, 1.6 MPa and 0.1 Hz, 2.7 Hz and 3 Hz. Lowest values for mag reflect 0.1 MPa.

The individual time sensitivity of each CA, γ_S^{CA}, consists of the product of two parameters; an adjustment factor (σ) and a CA-specific time sensitivity ($\gamma_{S,i}^{CA}$) (Eq. 2).

$$\gamma_S^{CA} = \sigma \cdot \gamma_{S,i}^{CA} \tag{2}$$

γ_S^{CA} within the anabolic range is referred to as $\gamma_{S,ana}^{CA}$ and within the catabolic range as $\gamma_{S,cata}^{CA}$. An approximation of σ to adjust numerically generated values to a biologically relevant range, as well as the details to obtain individual time sensitivities of mRNA expressions in NP cells, are provided in Methods.

Tackling the absence of a (fluctuating) stimulus. The relevance of representing a "zero" stimulus might be highly depending on the observed system of interest. Within the current system of interest of the NP, absence of the time-dependent stimulus "freq" is a physiological condition and represents static activities. Static activities are generally

deemed to be less anabolic than moderately dynamic activities (Chan et al., 2011), which required a particular consideration to duly represent the effect of static load. Its approximation is explained in Methods.

Qualitative validation of the PN_t-Methodology by calculating cell responses to microgravity and to various daily human activities. CA of each CS was calculated for optimal nutritional conditions (pH 7.1, 5 mM glc) (Nachemson, 1969; Rinkler et al., 2010). Two sets of simulations are provided; a first set of results encloses predictions for exposure to microgravity during six months of space flight compared to a corresponding time spent on Earth. A second set of results was obtained by simulating cell responses of non-inflamed cells for eight human physical activities: sleeping, sitting with an active or a round back, hiking with or without extra weight of 20 kg, walking, jogging and sitting in/on a motor vehicle. Results for the physical activities were provided both as a continuous evolution over 8 h and as an accumulation over 2 h. Details regarding the estimation of intradiscal pressures and freq and effective values for each calculated activity are explained in Methods (Table 4).

Calculations for an approximated daily life on Earth led to high CA in terms of mRNA expression of the functional structural proteins of the tissue (Agg, Col-II) and to (close to) minimal CA in terms of protease mRNA expression in non-inflamed cells. Inflammation caused an overall but modest upregulation of proteases and a slight downregulation of tissue proteins (Figure 5, A2).

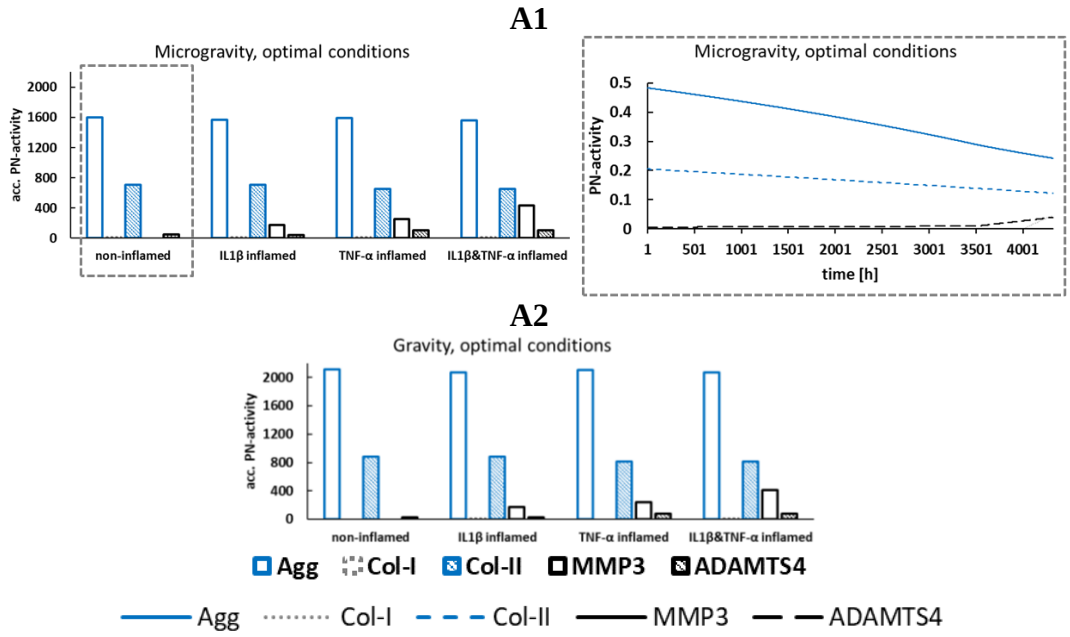

Figure 5: CA-profiles under microgravity: accumulated (acc.) PN-activity (A1, left) for four different proinflammatory cell states and the (continuous) PN-activity of non-inflamed cells (A1, right). CA-profiles of four different proinflammatory cell states (A2) for an approximated daily life on Earth. Time period: six months (180 days).

In contrast, exposure to microgravity (Figure 5, A1, left) led to an overall reduced PN-activity of the main tissue proteins to roughly 75% and 80% for Agg and Col-II mRNA expression, respectively. MMP3 mRNA expression was overall similar and ADAMTS4 was enhanced, though it remained low. The rise in ADAMTS4 protease expression could be especially attributed to the end of the stay in space (Figure 5, A1, right). Regarding specific physical activities (Figure 6), high anabolism was found for sleeping (Figure 6, B1, B2), sitting with an active back (Figure 6, B1, B3), walking (Figure 6, B1, B4) and walking without extra weight (Figure 6, B1, B5). Catabolic shifts were predicted for any other condition after either 1h or after prolonged exposure. Especially hiking with heavy weights (Figure 6, B1, B6) and exposure to vibration (Figure 6, B1, B9) appears to be critical, given that a catabolic shift was already expected within the first hour of stimulus exposure.

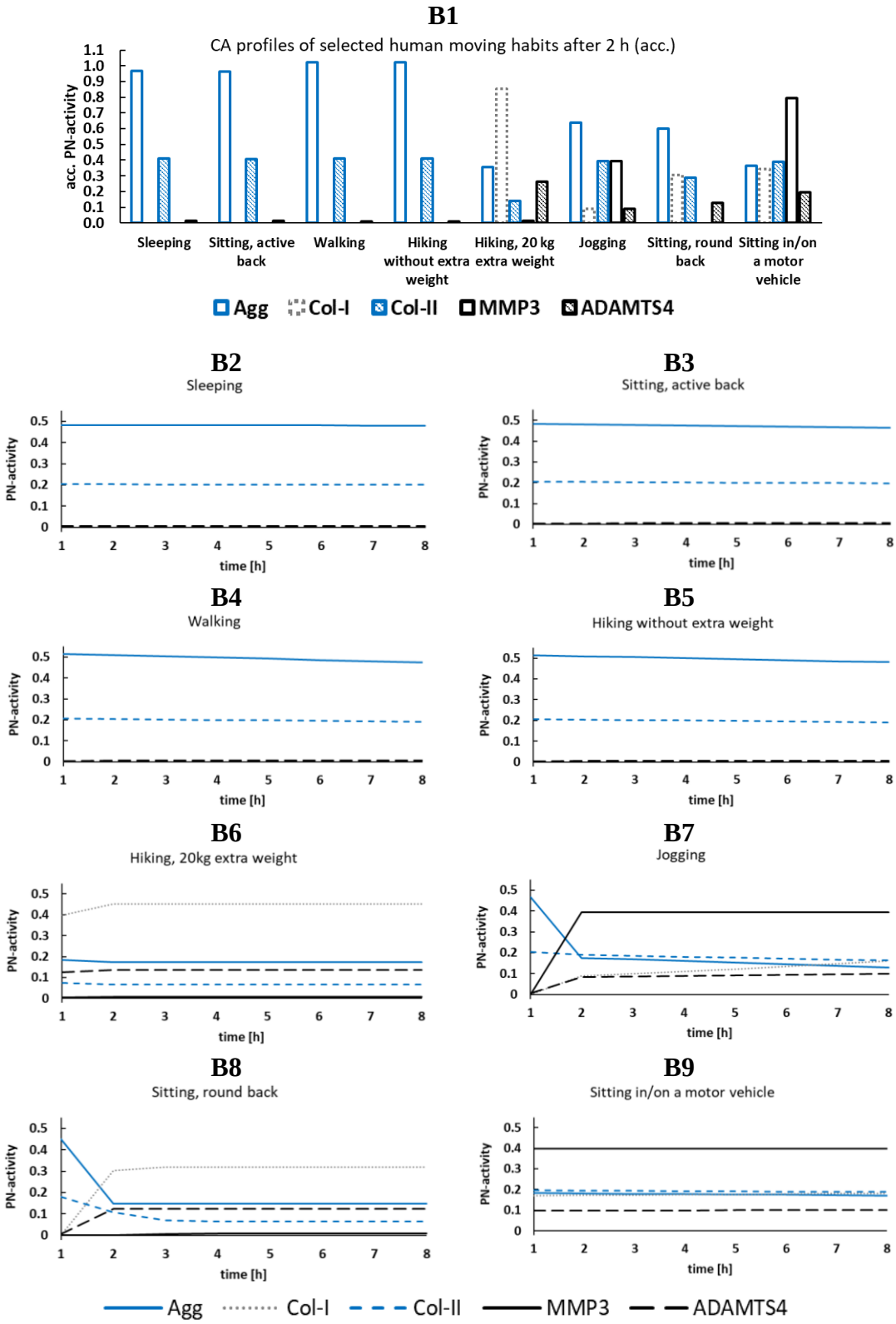

Figure 6: Predictions for eight selected physical activities: sleeping, walking, hiking with/without extra weight, jogging, sitting with an active/round back, exposure to vibration (as probably experienced by a motor vehicle). Accumulated (acc.) PN-activities after 2h (B1), and continuous PN-activities (B2-B9) over 8h of physical activity.

Discussion

The PN_t-Methodology reflects a high-level network modelling approach, where critical external and local stimuli were linked to relevant CA. Activations of different CA and CS were interpreted as parallel networks acting at the same time, and they were interrelated by the PN-equation. This novel top-down approach represents a strategy to evade the modeling of intracellular networks that often go along with limitations such as a loss of network directionality, difficulties in the calculation of unequivocal results or network overfitting. The PN_t-Methodology allows to approximate cellular responses to complex stimulus environments according to predictions of different experimental findings. By translating the quality of such findings into systems biology parameters, complex, dynamic multifactorial environments could be virtually approximated, including long time effects. Thereby, the systematic design of systems of interest promotes a systematic experimental investigation of stimulus - cell responses and points out the need for standardized experimental setups, in order to enhance comparability among experimental studies.

The PN_t-Methodology was designed to allow for a straightforward exchange of experimental input data. This was deemed to be a requirement to deal with the limited reproducibility of biological results due to differences in experimental protocols, high standard deviations, and low sample sizes. Hence, optimally, multiple sets of different input data would be run to interpret the results of the PN_t-Methodology rather stochastically than absolute, always when enough experimental data is available. Moreover, the data type, i.e. mRNA expression or protein synthesis, used to feed the system of interest, strongly depends on experimental availability. Accordingly, in this work, mRNA expressions were used. Given that mRNA expressions and protein

synthesis are not always proportional, additional calculations with a dataset about protein synthesis, would be instrumental to address the effect of CA on tissue remodeling in future. Such results could be used for multiscale top-down approaches, i.e. as feedback for intracellular network models.

Focus was set on a scalable design of the PN-equation that adapts to user-defined systems of interest. This is a requirement for both, a more extensive investigation of the current network and to enable the application of the PN_t-Methodology to multicellular systems of other tissues. Notably, compared to most other mathematical solutions, this methodology doesn't tackle the comparison to a reference value to assess activations (e.g. 1 in Boolean or fuzzy-logic approaches). This was particularly necessary to allow for the comparison of different CS. To achieve, however, a robust, relative comparability, the weight of each PN within the PN-system was assessed through weighting factors, that predefined the sensibility of each CA to the surrounding stimulus environment with respect to the sensibility of any other CA within the same PN-system.

An interesting aspect of approximating living, dynamic systems is the handling of the absence of a stimulus. In the simulated mechanosensitive multicellular system, this refers to the simulation of static conditions. In contrast to any other external stimulus considered in this multicellular system, freq is a stimulus, the absence of which is perfectly physiological. The absence of freq was found to be less anabolic than (moderate) dynamical behavior (Chan et al., 2011). Therefore, a discontinuity of the generic function towards 0 Hz must be assumed. Hence, the absence of freq was described as a special case, where the stimulus freq = 0 Hz was actively contributing to the response of a system (see Methods).

From a numerical point of view, one must bear in mind, that the non-linearity of the PN-equation favors the increase of PN-activities compared to decreases (Figure 8, Methods). Hence, tissue protein expressions decrease slowly, whilst the rise for proteases is more pronounced. The good qualitative findings of the current results (see Appendices 1 & 2) suggest that this tendency actually fits known biological dynamics in the NP of the IVD. Arguably, further work is required to test the performance of the PN_t-Methodology with the biology of other tissues.

Currently, the PN-equation only considers parallel effects of different stimuli, whilst possible cross-effects among different stimuli were not taken into consideration so far. Yet, the equation allows to introduce correction factors for stimulus interactions, e.g. by formulating the weighting factors as variables, in function of the surrounding stimulus environment, if experimental evidence points towards significant impacts of cross-effects. The quality of the model results by adding such an additional dimensionality remains to be investigated.

To integrate dose and time sensitivities, a mathematical description was developed to interrelate time dependency and stimulus dose. This was achieved through a generic function that relates the whole range of stimulus intensities to an either activating or inhibiting effect on a CA. Generic functions are based on general assumptions about the qualitative effect of a load on a CA. Hence, moderate loading conditions, in terms of both mag and freq, were generally assumed to be anabolic, and excessive loading was generally assumed to be catabolic. Thus, in addition to the overall data-driven approach presented here, this modelling approach allows to complement missing data by an integration of knowledge-driven data. Again here, the mathematical framework was

designed to allow for an easy adaptation of the generic functions in order to obtain more refined S-CA relationships as soon as corresponding information is available.

Relevant time-dependencies for the NP enclose a loss of anabolic stimulus over time and a time delay in the development of a catabolic response to a catabolic stimulus. The latter was programmed to take into consideration that short durations of high loading impacts might not promote IVD degeneration (Dudli et al., 2012), whilst sustained overload as such is considered as a risk factor for degenerative changes (Stokes and Iatridis, 2004). So far, time-dependencies were programmed to be gradual and linear and become non-linear due to an integration into the PN-equation. Despite the overall good qualitative results (Appendices 1 & 2), the effect of time might be non-linear and must be adapted as soon as further insights into the time-responses of cells is available. This might be done by reconsidering the time variable as a function.

Numerical incongruences for input data close to the α-β-threshold due to the continuous formulation of the generic functions are inevitable and discussed in the Appendix 3. Eventually, in this work time-dependencies were integrated to estimate the effect of mechanical stimuli. However, technically, they could also be programmed for biochemical stimuli.

This new methodology complements existing methodologies that cover the (sub) cellular- and tissue levels, focusing on an intermediate spatial scale. It allows to consider CA of different CS at locations of interest within a tissue. Input parameters could be obtained by Finite Element simulations at tissue /organ levels. Whilst this work focusses on cells of the same cell type for different CS, the PN_t-Methodology would technically allow to model heterogeneous cell types within a tissue, given that this top-down approach does not rely on cell type-specific intracellular pathways.

Further work should apply this novel approach to other tissues/diseases. This might include the assessment of the capacity to add active pharmaceutical ingredients as external stimuli to the system and investigate the response of different CA to this addition. Thereby, focus must be set to carefully choose a relevant system of interest on beforehand and to have the necessary experimental data available.

To the best of our knowledge, this is the first methodology that allows a straightforward approximation of relative cell responses within heterogeneous multifactorial, multicellular systems. Thanks to this novel top-down high-level network modelling approach based on experimental data and combined though an ODE, dynamic CA can be estimated over long periods of time with low computational costs, which is deemed to be an important step towards a better understanding of multifactorial disorders, such as IVD degeneration.

Methods

Determination of the weighting factors for mag and freq. To calculate the dose- and time-dependent impact of a stimulus, the corresponding weight of this stimulus (θ_S^{CA}) must be defined. Weighting factors were derived from changes in x-fold mRNA expressions (ϵ), converted into a "cellular effort" as previously explained (Baumgartner et al., 2021b). In short: The "cellular effort" allows to compare increases ($1 < \epsilon < \infty$) and decreases ($0 < \epsilon < 1$) of ϵ compared to a control level (1). Experimental data to approximate weighting factors for mag and freq were derived from a rat study, where NP cells were exposed to a mag of 1 MPa and three different frequencies of 0.01 Hz, 0.2 Hz and 1 Hz (MacLean et al., 2004). Weighting factors of mag were estimated using data of quasi-static conditions (i.e. 0.01 Hz). Weighting factors of freq were obtained

based on the maximal x-fold change in mRNA expression caused by the three aforementioned frequencies (Table 2).

Table 2: individual weighting factors for loading parameters.

Stimulus	**mRNA**	**Weighting factor (θ_S^{CA})**	**Experimental study**
Mag	Agg	0.3484	(MacLean et al., 2004)
	Col-I	0.8711	(MacLean et al., 2004)
	Col-II	0.1394	(MacLean et al., 2004)
	MMP3	0.0100	(MacLean et al., 2004)
	ADAMTS4	0.1394	(MacLean et al., 2004)
	TNF-α	0.0100	Indications(Dudli et al., 2012; Gawri et al., 2014)
	IL1β	0.0100	Indications(Walter et al., 2012)
Freq	Agg	0.3318	(MacLean et al., 2004)
	Col-I	0.4355	(MacLean et al., 2004)
	Col-II	0.0100	(MacLean et al., 2004)
	MMP3	0.5124	(MacLean et al., 2004)
	ADAMTS4	0.1048	(MacLean et al., 2004)
	TNF-α	0.0100	No information found
	IL1β	0.0100	No information found

According to experimental observations (Dudli et al., 2012; Gawri et al., 2014; Walter et al., 2012), the effect of mag on proinflammatory cytokine expression seems to be limited and information about the respective effect of freq was not found. Therefore, the weighting factors of TNF-α and IL1β was generally set to 0.01. A complete list of all weighting factors used in this study is provided in the Appendix 4.

Development of the PN_t-Methodology. The PN_t-Methodology is developed based on a well-established graph based method presented by Mendoza and Xenarios (Mendoza and Xenarios, 2006) (Eq. 3 & 4).

$$\frac{dx_i}{dt} = \frac{-e^{0.5h} + e^{-h(\omega_i - 0.5)}}{(1 - e^{0.5h})(1 + e^{-h(\omega_i - 0.5)})} - \gamma_i x_i \tag{3}$$

$$with$$

$$\omega_i = \left(\frac{1 + \sum \alpha_n}{\sum \alpha_n}\right)\left(\frac{\sum \alpha_n x_n^a}{1 + \sum \alpha_n x_n^a}\right)\left(1 - \left(\frac{1 + \sum \beta_m}{\sum \beta_m}\right)\left(\frac{\sum \beta_m x_m^i}{1 + \sum \beta_m x_m^i}\right)\right) \tag{4}$$

In short: Eq. 3 determines the overall activation of a node, x_i, where the gain variable (h) allows to gradually shape the relationship between $\frac{dx_i}{dt}$ and the total nodal input, ω_i, from a linear to a step function. The overall node activation can be reduced by integrating a decay rate (γ). Eq. 4 expresses the total input of the node, according to the set of activators x_n^a and inhibitors x_m^i that act on the node with the respective positive strengths α_n and β_m (Figure 7, A). Nodal activation is always bound between 0 and 1.

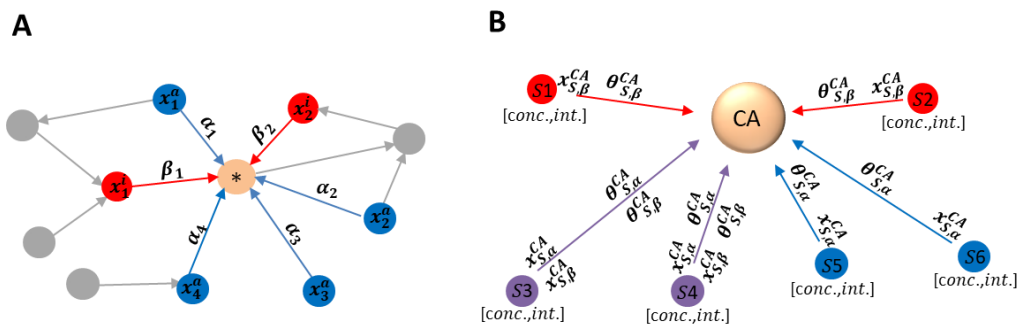

$0 \leq x_n^a, x_m^i, \leq 1 \quad \alpha_n, \beta_m > 0 \qquad 0 \leq x_S^{CA} \leq 1 \quad 0.01 \leq \theta_S^{CA} \leq 1$

Figure 7: Comparison between the network presented by Mendoza and Xenarios 2006 (Mendoza and Xenarios, 2006) (A) and the concept of parallel network modelling to tackle heterogeneous stimulus environments (B), where an individual parallel network for a given stimulus environment of six stimuli is shown. The overall activity of the principal node (* vs. CA) is determined by adjacent network nodes (A), or by a local stimulus environment (B). The effect of adjacent nodes is either activating (blue, α) or inhibiting (red, β) (A, B) or includes dose and time dependencies (B, purple; S3, S4). Whilst network nodes are usually interconnected within each other (A), the objective of individual parallel networks (B) is to determine a final CA. $\boldsymbol{\alpha_n}, \boldsymbol{\beta_m}, \boldsymbol{\theta_S^{CA}}$: activating/inhibiting factors. $\boldsymbol{x_n^a}, \boldsymbol{x_m^i}, \boldsymbol{x_S^{CA}}$: adjacent node activation (A), normalized stimulus dose, i.e. concentration (conc.) /intensity (int.) (B).

A PN-network is always directional as it reflects the effect of adjacent nodes on one principal node that stands for a CA (Figure 7, B). Adjacent nodes represent the stimulus (micro-) environment. The impact of each adjacent node is determined by the product of a weighting factor (θ_S^{CA}) and the corresponding stimulus concentration/intensity (x_S^{CA}) (Figure 2, B, Results). Moreover, the integration of time- and dose-dependencies within the PN-network allows a stimulus to be either activating or inhibiting, according to the user-defined stimulus dose and the time, during which the condition is maintained.

Within the PN_t-Methodology, the decay term defined by Mendoza & Xenarios (Eq. 3) would reflect a possible decay in mRNA expression under sustained stimulation or the half-life of a secreted protein. In the present methodology the decay terms would represent, however, an additional source of uncertainty, and they don't add further information about the regulation of the system of interest and were, therefore, not considered. Moreover, given that CA are directly obtained through the S-CA relationships that are based on experimental findings, no additional manipulation of ω_i is needed, i.e. h in Eq. 3 reflects a linear relationship between $\frac{dx_i}{dt}$ and the total nodal input ω_i in the PN_t-Methodology. Accordingly, the overall CA was directly assessed by ω_i, leading to Eq. 5.

$$\frac{dx_i}{dt} = \omega_i \tag{5}$$

The activating portion of the PN-equation. The activating portion of the PN-equation (Eq. 1) determines an overall activation of a CA relative to any other CA within the same PN-system. Hence, within the term $\left(\frac{1+\sum\theta_\alpha}{\sum\theta_\alpha}\right)$, all activating weighting factors of the tackled PN-system were considered, which determines its size. The second fraction of the activating term defines the activation of each individual network, by $\sum\theta_{S,\alpha}^{CA}x_{S,\alpha}^{CA}$. Thus, the maximal activation of a CA is determined by $\sum\theta_{S,\alpha}^{CA}$, i.e. with $x_{S,\alpha}^{CA} = 1$.

Given the non-linearity of the approach, values of maximal activations strongly depend on the pre-established size of the PN-system. Thereby, the maximal activation of one PN-network reflects a fraction of the overall size of the PN-system, i.e. $\sum \theta_{S,\alpha}^{CA} = \lambda \sum \theta_\alpha$ with $0 < \lambda \leq 1$. Hence, λ describes the relative weight of one parallel network within the PN-system. Thus, $\lambda = 1 \rightarrow \sum \theta_{S,\alpha}^{CA} = \sum \theta_\alpha$ would reflect a reduction of the system to just one parallel network. In contrast, maximal activations of individual networks decrease with increasing PN-systems, and the results, i.e. the overall CA ($\frac{d\omega_{CA,CS}}{dt}$, Eq.1) of individual networks require a high resolution, reflected in elevated decimal places. To cope with this, the first fraction of the activating term is designed to assign higher relative weights to individual parallel networks with increasing sizes of PN-systems (Figure 8).

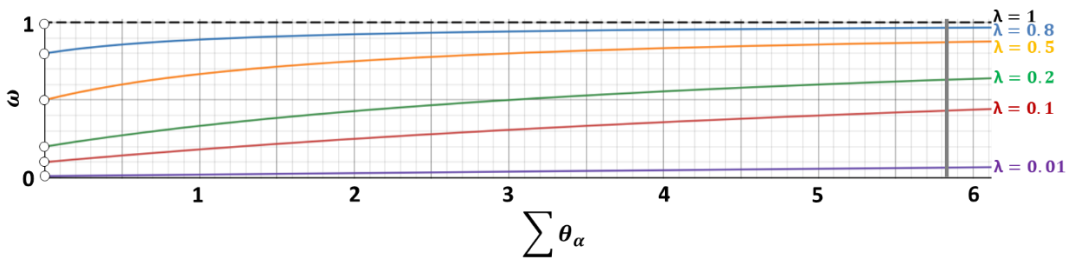

$$\omega_{max} = \frac{1 + \sum \theta_\alpha}{\sum \theta_\alpha} \cdot \frac{(\lambda \sum \theta_\alpha)}{1 + (\lambda \sum \theta_\alpha)} \; with \; 0 < \lambda \leq 1 \quad and \; \lambda \sum \theta_\alpha = \sum \theta_{S,\alpha}^{CA}$$

Example: Agg, non−inflamed cells:

$\sum \theta_{S,\alpha}^{Agg} = 0.7844, \lambda_{Agg}=0.1344*, \omega_{max,Agg}=0.5149*$

*rounded

Size, current PN-system: $\sum \theta_\alpha = 5.8337$

Estimation for different $x_{S,\alpha}^{CA}$:

$$\omega = \frac{1 + \sum \theta_\alpha}{\sum \theta_\alpha} \cdot \frac{((\lambda \sum \theta_\alpha) \cdot x_{S,\alpha}^{Agg})}{(1 + (\lambda \sum \theta_\alpha) \cdot x_{S,\alpha}^{Agg})}$$

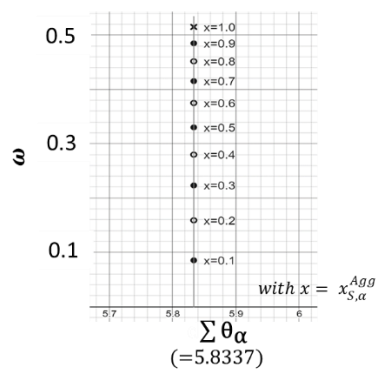

Figure 8: Evolution of the relative size of a parallel network with an increasing size of the PN-system. Exemplary relative sizes of individual networks are plotted (λ= 1, λ = 0.8, λ =0.2, λ =0.1, λ =0.01). Specific values for Aggrecan (Agg) of the current PN-system of the NP were exemplarily shown. The size of the PN-system is 5.8337 and marked as a grey bar within the plot. The effect of different values for $\boldsymbol{x_{S,\alpha}^{CA}}$ i.e. from x=0.1 to x=1.0, was plotted for Agg. ω is not defined for $\sum \boldsymbol{\theta_\alpha} = \mathbf{0}$.

Eventually, the PN-equation assigns an individual range to each CA, in which it varies according to its $x_{S,\alpha}^{CA}$ and its individual inhibition. The nonlinear behavior of the PN-equation due to different values of $x_{S,\alpha}^{CA}$ is schematically represented (Figure 8).

The inhibiting portion of the PN-equation. The inhibiting portion of the PN-equation lowers the current activation of a CA and is defined relative to the activation of the CA. The first fraction determines the relative weight of the inhibition on the CA. Hence, if the activation of a CA was determined based on weak activators and powerful inhibitors, the impact of inhibition was strong and vice versa. Importantly, this term prevents weak inhibitors to completely erase overall cell activations.

The second inhibiting fraction defines the maximal inhibition of a CA by considering all the different CS of a CA. This allows for coherent inhibiting impacts of different CS. Hence, its function is equivalent to the first activating fraction of the PN-equation, but instead of considering the whole PN-system, only different CS of the same CA were considered.

The third fraction of the inhibiting term determines the actual weight of the inhibition, analogue to the second fraction of the activating term (Figure 9).

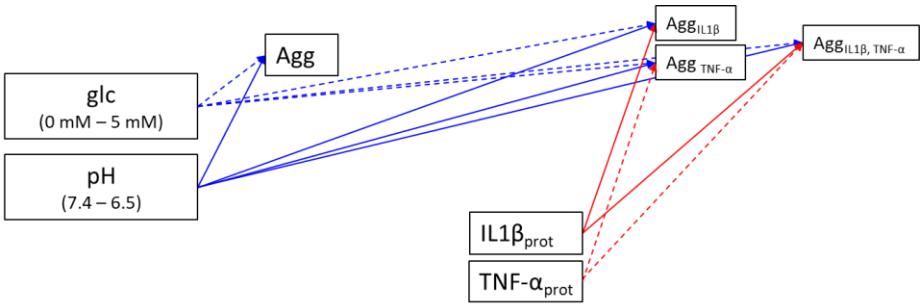

$$\frac{d\omega_{\mathrm{Agg,non-infl}}}{dt} = \left(\left(\frac{1+\sum\theta_{\alpha}}{\sum\theta_{\alpha}}\right)\left(\frac{\sum\theta_{S,\alpha}^{Agg}x_{S,\alpha}^{Agg}}{1+\sum\theta_{S,\alpha}^{Agg}x_{S,\alpha}^{Agg}}\right)\right) = \alpha_{Agg}$$

$$\frac{d\omega_{\mathrm{Agg,IL1\beta\ infl}}}{dt} = \alpha_{Agg}\cdot\left(1-\left(\left(\frac{\theta_{IL1\beta,\beta}^{Agg}}{\theta_{\mathrm{glc},\alpha}^{Agg}+\theta_{\mathrm{pH},\alpha}^{Agg}+\theta_{IL1\beta,\beta}^{Agg}}\right)\left(\left(\frac{1+\theta_{IL1\beta,\beta}^{Agg}+\theta_{TNF-\alpha,\beta}^{Agg}}{\theta_{IL1\beta,\beta}^{Agg}+\theta_{TNF-\alpha,\beta}^{Agg}}\right)\left(\frac{\theta_{IL1\beta,\beta}^{Agg}x_{IL1\beta,\beta}^{Agg}}{1+\theta_{IL1\beta,\beta}^{Agg}x_{IL1\beta,\beta}^{CA}}\right)\right)\right)\right)$$

$$\frac{d\omega_{\mathrm{Agg,TNF-\alpha\ infl}}}{dt} = \alpha_{Agg}\cdot\left(1-\left(\left(\frac{\theta_{TNF-\alpha,\beta}^{Agg}}{\theta_{\mathrm{glc},\alpha}^{Agg}+\theta_{\mathrm{pH},\alpha}^{Agg}+\theta_{TNF-\alpha,\beta}^{Agg}}\right)\left(\left(\frac{1+\theta_{IL1\beta,\beta}^{Agg}+\theta_{TNF-\alpha,\beta}^{Agg}}{\theta_{IL1\beta,\beta}^{Agg}+\theta_{TNF-\alpha,\beta}^{Agg}}\right)\left(\frac{\theta_{TNF-\alpha,\beta}^{Agg}x_{TNF-\alpha,\beta}^{Agg}}{1+\theta_{TNF-\alpha,\beta}^{Agg}x_{TNF-\alpha,\beta}^{Agg}}\right)\right)\right)\right)$$

$$\frac{d\omega_{\mathrm{Agg,IL1\beta\&TNF-\alpha\ infl}}}{dt} = \alpha_{Agg}\cdot\left(1-\left(\left(\frac{\theta_{IL1\beta,\beta}^{Agg}+\theta_{TNF-\alpha,\beta}^{Agg}}{\theta_{\mathrm{glc},\alpha}^{Agg}+\theta_{\mathrm{pH},\alpha}^{Agg}+\theta_{IL1\beta,\beta}^{Agg}+\theta_{TNF-\alpha,\beta}^{Agg}}\right)\left(\left(\frac{1+\theta_{IL1\beta,\beta}^{Agg}+\theta_{TNF-\alpha,\beta}^{Agg}}{\theta_{IL1\beta,\beta}^{Agg}+\theta_{TNF-\alpha,\beta}^{Agg}}\right)\left(\frac{\theta_{IL1\beta,\beta}^{Agg}x_{IL1\beta}^{Agg}+\theta_{TNF-\alpha,\beta}^{Agg}x_{TNF-\alpha,\beta}^{Agg}}{1+\theta_{IL1\beta,\beta}^{Agg}x_{IL1\beta}^{CA}+\theta_{TNF-\alpha,\beta}^{Agg}x_{TNF-\alpha,\beta}^{Agg}}\right)\right)\right)\right)$$

Figure 9: Illustration of the determination of the inhibiting part of the PN equation (here, the inhibition is caused by the impact of IL1β and TNF-α proteins (prot), respectively) . Example for the different CS of Aggrecan (Agg) exposed under the influence of glc and pH. Analogue formulations between the activating and inhibiting terms were indicated with dotted lines. Infl: inflamed

An example of a complete PN-equation. Subsequently, an example of a complete PN-equation of the PN-system I of the system of interest of the NP (Figure 2, A) is shown for the Agg mRNA expression of IL1β-inflamed cells, for an initially anabolic mag and catabolic freq (Figure 10).

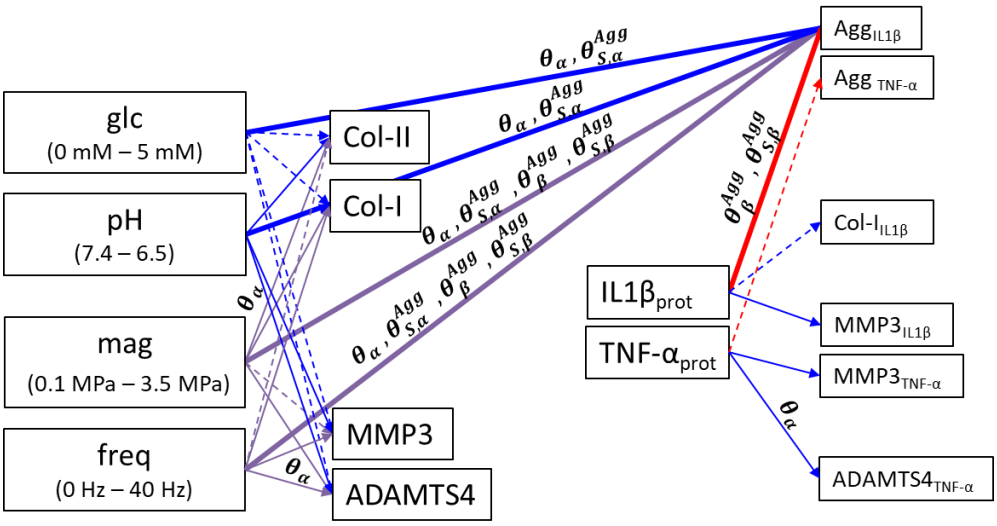

θ_α: all (potentially) activating weighting factors within the PN-System
$\theta_{S,\alpha}^{Agg}$: activating weighting factors that are directly acting on Agg of IL1β inflamed cells
θ_{β}^{Agg}: all (potentially) inhibiting weighting factors of Agg, independently of the CS
$\theta_{S,\beta}^{Agg}$: inhibiting weighting factors that are directly acting on Agg of IL1β inflamed cells

$$\frac{d\omega_{Agg,\,IL1\beta\,infl}}{dt} = \left(\left(\frac{1+\sum\theta_\alpha}{\sum\theta_\alpha}\right)\left(\frac{\theta_{glc,\alpha}^{Agg}x_{glc,\alpha}^{Agg}+\theta_{pH,\alpha}^{Agg}x_{pH,\alpha}^{Agg}+\theta_{mag,\alpha}^{Agg}x_{mag,\alpha}^{Agg}}{1+\theta_{glc,\alpha}^{Agg}x_{glc,\alpha}^{Agg}+\theta_{pH,\alpha}^{Agg}x_{pH,\alpha}^{Agg}+\theta_{mag,\alpha}^{Agg}x_{mag,\alpha}^{Agg}}\right)\right)\cdot$$
$$1-\left(\left(\frac{\theta_{\delta,mag,\beta}^{Agg}+\theta_{freq,\beta}^{Agg}+\theta_{IL1\beta,\beta}^{Agg}}{(\boldsymbol{\theta_{glc,\alpha}^{Agg}}+\boldsymbol{\theta_{pH,\alpha}^{Agg}})+(\boldsymbol{\theta_{\delta,mag,\beta}^{Agg}}+\boldsymbol{\theta_{IL1\beta,\beta}^{Agg}}+\boldsymbol{\theta_{freq,\beta}^{Agg}})}\right)\cdot\left(\frac{1+\theta_{\delta,mag,\beta}^{Agg}+\theta_{freq,\beta}^{Agg}+\theta_{IL1\beta,\beta}^{Agg}+\theta_{TNF-\alpha,\beta}^{Agg}}{\theta_{\delta,mag,\beta}^{Agg}+\theta_{freq,\beta}^{Agg}+\theta_{IL1\beta,\beta}^{Agg}+\theta_{TNF-\alpha,\beta}^{Agg}}\right)$$
$$\cdot\left(\frac{\theta_{\delta,mag,\beta}^{Agg}x_{mag,\beta}^{Agg}+\theta_{freq,\beta}^{Agg}x_{freq,\beta}^{Agg}+\theta_{IL1\beta,\beta}^{Agg}x_{IL1\beta,\beta}^{Agg}}{1+\theta_{\delta,mag,\beta}^{Agg}x_{mag,\beta}^{Agg}+\theta_{freq,\beta}^{Agg}x_{freq,\beta}^{Agg}+\theta_{IL1\beta,\beta}^{Agg}x_{IL1\beta,\beta}^{Agg}}\right)\Bigg) \qquad (6)$$

with

$$\sum\theta_\alpha = \theta_{glc}^{Agg}+\theta_{pH}^{Agg}+\theta_{glc}^{ColII}+\theta_{pH}^{ColII}+\theta_{glc}^{ColI}+\theta_{pH}^{ColI}+\theta_{glc}^{MMP3}+\theta_{pH}^{MMP3}+\theta_{glc}^{ADAMTS4}+\theta_{pH}^{ADAMTS4}+\theta_{IL1\beta}^{ColI}+\theta_{IL1\beta}^{MMP3}$$
$$+\theta_{TNF-\alpha}^{MMP3}+\theta_{TNF-\alpha}^{ADAMTS4}+\theta_{mag}^{Agg}+\theta_{freq}^{Agg}+\theta_{mag}^{ColII}+\theta_{freq}^{ColII}+\theta_{mag}^{ColI}+\theta_{freq}^{ColI}+\theta_{mag}^{MMP3}+\theta_{freq}^{MMP3}+\theta_{mag}^{ADAMTS4}+\theta_{freq}^{ADAMTS4}$$

Figure 10: Above: PN-equation for the Agg mRNA expression of IL1β inflamed cells. Every possible contribution of the weighting factors is illustrated. $\boldsymbol{\theta_\alpha}$ is illustratively represented in the PN-system but stands for all potentially activating S-CA relationships, see $\sum\boldsymbol{\theta_\alpha}$ of the equation. Below: Eq. 6 reflecting the Agg mRNA expression under an initially anabolic mag and catabolic freq. $\boldsymbol{\delta}$ reflects completive weighting factors.

Note that time-dependent weighting factors must be mentioned only once in the denominator of the first inhibiting term (Figure 10, bold), to accurately reflect the relative weight of inhibition with respect to activation.

PN-systems associated with the local stimuli IL1β and TNF-α (PN-systems II & III, in Figure 2, A). Given that no interrelated response to the targeted protein and protease

mRNA expressions are required (PN-system I, see Figure 2, A), and that proinflammatory cytokine expressions were required to feed the inflammation submodel (Baumgartner et al., 2021b), they were considered as separate PN-systems (PN-systems II & III). Hence, both PN-systems II and III only contain one parallel network each. Therefore, the first fraction of the activating part of the PN-equation for the PN-systems II and III only considers the weighting factors related to the specific CA (i.e. the CA for the mRNA expressions of the local stimuli IL1β and TNF-α). Eq. 7 shows the PN-equation for TNF-α:

$$\frac{d\omega_{TNF-\alpha,CS}}{dt} = \left(\left(\frac{1+\theta_{glc,\alpha}^{TNF-\alpha}+\theta_{pH,\alpha}^{TNF-\alpha}+\theta_{(\delta),mag,\alpha}^{TNF-\alpha}+\theta_{(\delta),freq,\alpha}^{TNF-\alpha}}{\theta_{glc,\alpha}^{TNF-\alpha}+\theta_{pH,\alpha}^{TNF-\alpha}+\theta_{(\delta),mag,\alpha}^{TNF-\alpha}+\theta_{(\delta),freq,\alpha}^{TNF-\alpha}}\right)\left(\frac{\sum\theta_{S,\alpha}^{CA}x_{S,\alpha}^{CA}}{1+\sum\theta_{S,\alpha}^{CA}x_{S,\alpha}^{CA}}\right)\right) \cdot \left(1-\left(\left(\frac{\sum\theta_{S,\beta}^{CA}}{\sum\theta_{S,\alpha}^{CA}+\sum\theta_{S,\beta}^{CA}}\right)\left(\left(\frac{1+\sum\theta_{\beta}^{CA}}{\sum\theta_{\beta}^{CA}}\right)\left(\frac{\sum\theta_{S,\beta}^{CA}x_{S,\beta}^{CA}}{1+\sum\theta_{S,\beta}^{CA}x_{S,\beta}^{CA}}\right)\right)\right)\right) \quad (7)$$

Determination of relevant stimulus ranges and specific logistic functions for mag and freq. Relevant, stimulus levels for mag were determined based on *in vivo* studies and range from 0.1 MPa to 3.5 MPa (Nachemson and Elfström, 1970; Wilke et al., 1999). Hence, in this approach, mag refers to intradiscal pressures. The range for freq was set to 0 Hz – 40 Hz, aiming to allow predictions for the effect of whole body exposures to high-frequency in daily occasions. The minimal step size for both, mag and freq was set to 0.05. To estimate the shape of the functions, *in vivo* and *in vitro* data and knowledge were used to assign different levels of mag and freq to anabolic or catabolic cell responses (Chan et al., 2011; Kasra et al., 2006; Nachemson and Elfström, 1970; Pachi and Ji, 2005; Vernillo et al., 2017; Walsh and Lotz, 2004; Wilke et al., 1999). In case of the generic function of mag, low and moderate pressures due to e.g. lying or walking were assumed to be highly anabolic. With rising intradiscal pressures,

as obtained during jogging, anabolism lowers until the stimulus becomes catabolic. Additionally, findings from Chan, Ferguson, and Gantenbein-Ritter (Chan et al., 2011) were considered that suggest that magnitudes around 0.2 MPa and 0.8 MPa reflect a potentially beneficial range of magnitude, whereas a (static) compression loading of >1 MPa induced degenerative changes. The generic functions for freq were set assuming walking freq to be overall beneficial. Walking freq might include freq of up to around 2.5 Hz as observed by (Pachi and Ji, 2005). In contrast, freq of 3-8 Hz, or over a threshold of 5 Hz, possibly disrupt proper cell function (Kasra et al., 2006). The functions were fitted to an accuracy of four decimals, in agreement with the fitting of the continuous functions that describe the effect of nutrition-related stimuli (Figure 2, B), as previously explained (Baumgartner et al., 2021b). The mathematical formulation of the four generic functions are presented in Eq. 8-11.

$$X_{Mag}^{A;I} = -\frac{e^{14mag} \cdot 1.99999}{e^{14mag} + 1.2 \cdot 10^6} + \frac{1.99999}{2} \tag{8}$$

$$X_{Mag}^{I;A} = \frac{e^{14mag} \cdot 1.99999}{e^{14mag} + 1.2 \cdot 10^6} - \frac{1.99999}{2} \tag{9}$$

$$X_{Freq}^{A;I} = -\frac{e^{6freq} \cdot 1.99999}{e^{6freq} + 6.6 \cdot 10^7} + \frac{1.99999}{2} \tag{10}$$

$$X_{Freq}^{I;A} = \frac{e^{6freq} \cdot 1.99999}{e^{6freq} + 6.6 \cdot 10^7} - \frac{1.99999}{2} \tag{11}$$

Estimation of individual time sensitivities of mRNA expressions in NP cells. $\gamma_{S,i,ana}^{CA}$ was estimated based on experimental data, where the effect of 1 MPa and 1 Hz on rat NP cells was assessed after 0.5h, 2h and 4h (MacLean et al., 2005). Thereby, the ratio of a mathematically assessed “cellular effort” was used (Baumgartner et al., 2021b) as done for the determination of the weighting factors for mag and freq. $\gamma_{S,i,cata}^{CA}$ was derived from the values assessed for $\gamma_{S,i,ana}^{CA}$ and Agg was chosen as a reference value (1) to determine the individual time delays of CA to unfold their whole catabolic

potential. Time sensitivities within the catabolic range for any other CA were obtained as fractions, relative to Agg (Table 3).

Table 3: individual time sensitivities for initially anabolic (ana) and catabolic (cata) stimulus intensities. Agg was used as a reference for the determination of catabolic time sensitivities.

CA	$\gamma^{CA}_{mag,i,ana}/\gamma^{CA}_{freq,i,ana}$	$\gamma^{CA}_{mag,i,cata}/\gamma^{CA}_{freq,i,cata}$
Agg (ref)	3.1429	1
Col-II	1.7500	$\frac{1.7500}{3.1429} = 0.5568$
Col-I	2.7647	$\frac{2.7647}{3.1429} = 0.8797$
MMP3	2.1571	$\frac{2.1571}{3.1429} = 0.6864$
ADAMTS4	3.1481	$\frac{3.1481}{3.1429} = 1.0017$
TNF-α	0.3143	No catabolic time sensitivity
IL1β	0.3143	No catabolic time sensitivity

With regard to the proinflammatory cytokines, no information about a possible time-sensitivity to loading conditions was found. Therefore, initially prudent time sensitivities were chosen for $\gamma^{CA}_{S,i,ana}$, being 10 times lower than the time sensitivity of Agg. This assumption was based on the observation that long-term exposure to microgravity does not categorically lead to IVD failure (Belavy et al., 2016), whereas excessive inflammatory conditions might provoke non recoverable catabolic shifts (Purmessur et al., 2013). Under initially catabolic loading, no time-delay was programmed, thus, values provided by the generic function were used to determine the inflammatory environment (Table 3).

Estimation of the adjustment factor (σ) to approximate mRNA expressions in NP cells. To estimate σ, it was supposed that 8h of axial dynamic loading of 0.2-0.8 MPa

and 0.1-1 Hz may not induce degeneration of the disc (Chan et al., 2011). Hence, model predictions for 0.2 MPa and 0.8 MPa at a medium freq of 0.5 Hz were calculated for adjustment factors of $\sigma = 1$ to $\sigma = 4$ (non-inflamed cells, under optimal, nutritional conditions of 5 mM glc, pH 7.1) and results were evaluated with regard to their catabolic progression at 0.8 MPa (Figure 11).

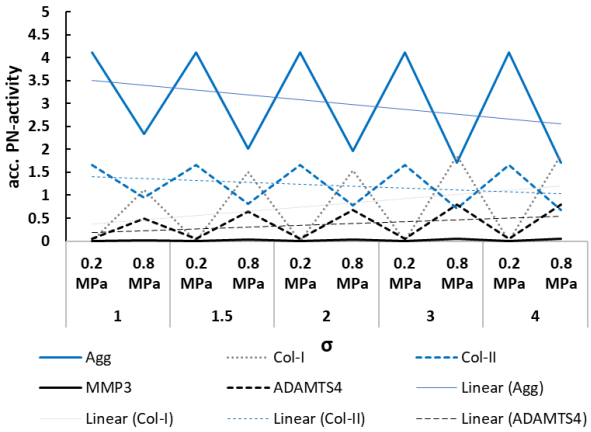

Figure 11: model predictions for different adjustment factors ($\boldsymbol{\sigma}$) and corresponding tendencies. Optimal nutritional conditions (5 mM glc, pH 7.1) and a frequency of 0.5 Hz were used.

Results showed that catabolic predictions at 0.8 MPa were already elevated for $\sigma = 2$. This is reflected by a higher acc. PN-activity for Col-I than Col-II, a considerably lower Agg mRNA expression compared to $\sigma = 1$ and a close approximation of the CA of Col-II and ADAMTS4. Hence, as an initial approximation for an adjustment factor, a medium value between $\sigma = 1$ and $\sigma = 2$, i.e. $\sigma = 1.5$ was set.

Estimation of the effect of the absence of freq. To consider static loading, the impact of "no-frequency" on a CA must be estimated. Therefore, the assumption that degeneration might not be induced during 8h dynamic axial loading with a load of 0.2 - 0.8 MPa and 0.1-1 Hz (Chan et al., 2011) was used. Hence, a dynamic daily human physical activity with loading parameters within the suggested range was compared to a

generally anabolic, static, human behavior. As a dynamic human moving activity, comfortable walking ("hiking") was chosen. It was approximated by a mag of 0.60 MPa, reflecting a (rounded) average intradiscal pressure during walking (Wilke et al., 1999), and a freq of 1.00 Hz. The static control was chosen to be "sleeping", reflected by an intradiscal pressure of 0.15 MPa, being the (rounded) average intradiscal pressure during night, over a period of 7h (Wilke et al., 1999). Agg was chosen as the reference protein for the fitting (Figure 12).

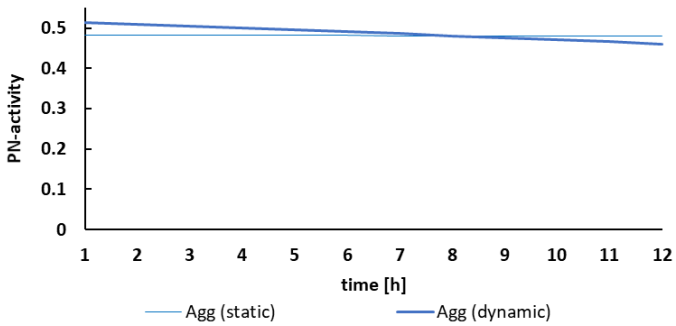

Figure 12: Illustration of the model prediction with $\boldsymbol{X_{freq,0}} = \boldsymbol{0.75}$ for Agg (ref).

Results showed that, a loss of anabolism due to dynamic loading compared to a static control after 8h was approximated with $X_{freq,0} = 0.75$. An example for Agg: within the first hour of an anabolic static condition, e.g. sitting, the x_{freq}^{Agg} contributes to the overall activation with a value of 0.75, which then continuously decreased due to time dependency. The time dependency for static loading was defined using the generic function of freq at 0 Hz as explained in Results.

Qualitative validation of the PN_t-Methodology: simulation of exposure to microgravity and physical activities. The duration of exposure to microgravity was derived from expeditions to the International Space Station (ISS) launched by the NASA (NASA, 2011). The effect of exposure to microgravity was compared to the effect calculated through an approximation of a corresponding time spent on Earth. An

average day was thereby distributed in 10h sleeping/laying down (night/day rest), two episodes of 4h sedentary work (sitting) and roughly three episodes of 2h physical activity (walking). Hence, the simulated day reflects quite an optimal human moving behavior. The period of time, during which a physical activity is carried out matters for calculation purposes: the day is represented by the additive effects of different activities. The time-step of calculation was 1h, thus, the CA was estimated after each hour of a certain physical activity. Accumulated CA after one day were then multiplied over 180 days. Simulations for four different CS (non-inflamed and inflamed for TNF-α, IL1β and both, TNF-α&IL1β) were provided (see Results and Appendix 2).

Intradiscal pressures for both, exposure to microgravity and physical activities were obtained from in-vivo measurements (Wilke et al., 1999) and rounded to the minimal step size of loading parameters (i.e. 0.05). Whenever intradiscal pressures were provided as ranges, average values were used for the simulation (e.g. walking: 0.53 MPa – 0.65 MPa (Wilke et al., 1999)). For microgravity calculations, the intradiscal pressure reflected the (rounded) value after 7h of rest (Wilke et al., 1999). Freq for hiking was reasonably estimated to be around 1 Hz, whilst values for walking and jogging were within the range as found in observational studies (Pachi and Ji, 2005; Vernillo et al., 2017). A vibration for “sitting in/on a motor vehicle” was estimated within the range of maximal catabolic predictions. An overview of the simulated human activities with corresponding loading parameters and duration is provided in Table 4.

Table 4: overview of the simulated human activities, corresponding loading parameters magnitude (mag) and frequency (freq), and duration (h)

Human activity			mag [MPa]	freq [Hz]	time [h]
Microgravity			0.25	-	4320
Average day on Earth		Sleeping / laying down	0.15	-	10
		Sitting with an active back	0.55	-	2x4
		Walking	0.60	1.80	3x2
Daily physical activities					
	1	Sleeping	0.15	-	2;8
	2	Sitting, active back	0.55	-	2;8
	3	Sitting, round back	0.85	-	2;8
	4	Hiking without extra weight	0.60	1.00	2;8
	5	Hiking, 20kg extra weight	1.10	1.00	2;8
	6	Walking	0.60	1.80	2;8
	7	Jogging	0.65	2.75	2;8
	8	Sitting in/on a motor vehicle	0.55	15.00	2;8

ACKNOWLEDGEMENTS

This work was supported by the European Commission (Disc4All-MSCA-2020-ITN-ETN 955735), by the Department of Information and Communication Technologies of the Universitat Pompeu Fabra and by the Spanish Ministry of Science and Innovation and State Agency for Research (STRATO-PID2021-126469OB-C21).

COMPETING INTERESTS

The authors declare no competing interests.

REFERENCES

Aldridge BB, Saez-Rodriguez J, Muhlich JL, Sorger PK, Lauffenburger DA. 2009. Fuzzy Logic Analysis of Kinase Pathway Crosstalk in TNF/EGF/Insulin-Induced Signaling. *PLoS Comput Biol* **5**:e1000340. doi:10.1371/journal.pcbi.1000340

Bailey JF, Miller SL, Khieu K, O´Neill CW, Healey RM, Coughlin DG, Sayson J V., Chang DG, Hargens AR, Lotz JC. 2018. From the international space station to the clinic: how prolonged unloading may disrupt lumbar spine stability. *Spine J* **18**:7–14. doi:10.1016/j.spinee.2017.08.261

Baumgartner L, Reagh JJ, González Ballester MA, Noailly J. 2021a. Simulating intervertebral disc cell behaviour within 3D multifactorial environments. *Bioinformatics* **37**:1246–1253. doi:10.1093/bioinformatics/btaa939

Baumgartner L, Sadowska A, Tío L, González Ballester MA, Wuertz-Kozak K, Noailly J. 2021b. Evidence-based Network Modelling to Simulate Nucleus Pulposus Multicellular Activity in different Nutritional and pro-Inflammatory Environments. *Front Bioeng Biotechnol* **9**:1–17. doi:10.3389/fbioe.2021.734258

Baumgartner L, Wuertz-Kozak K, Le Maitre CL, Wignall F, Richardson SM, Hoyland J, Wills CR, González Ballester MA, Neidlin M, Alexopoulos LG, Noailly J. 2021. Multiscale regulation of the intervertebral disc: Achievements in experimental, in silico, and regenerative research. *Int J Mol Sci* **22**:703. doi:10.3390/ijms22020703

Belavy DL, Adams M, Brisby H, Cagnie B, Danneels L, Fairbank J, Hargens AR, Judex S, Scheuring RA, Sovelius R, Urban J, van Dieën JH, Wilke HJ. 2016. Disc herniations in astronauts: What causes them, and what does it tell us about herniation on earth? *Eur Spine J* **25**:144–154. doi:10.1007/s00586-015-3917-y

Belavý DL, Quittner MJ, Ridgers N, Ling Y, Connell D, Rantalainen T. 2017. Running exercise strengthens the intervertebral disc. *Sci Rep* **7**:1–8. doi:10.1038/srep45975

Chan SCW, Ferguson SJ, Gantenbein-Ritter B. 2011. The effects of dynamic loading on the intervertebral disc. *Eur Spine J* **20**:1796–1812. doi:10.1007/s00586-011-1827-1

Dudli S, Haschtmann D, Ferguson SJ. 2012. Fracture of the vertebral endplates, but not equienergetic impact load, promotes disc degeneration in vitro. *J Orthop Res* **30**:809–816. doi:10.1002/jor.21573

Garcia KM, Harrison MF, Sargsyan AE, Ebert D, Dulchavsky SA. 2018. Real-time Ultrasound Assessment of Astronaut Spinal Anatomy and Disorders on the International Space Station. *J Ultrasound Med* **37**:987–999. doi:10.1002/jum.14438

Gawri R, Rosenzweig DH, Krock E, Ouellet JA, Stone LS, Quinn TM, Haglund L. 2014. High mechanical strain of primary intervertebral disc cells promotes secretion of inflammatory factors associated with disc degeneration and pain. *Arthritis Res Ther* **16**:R21. doi:10.1186/ar4449

Gilbert HTJ, Hodson N, Baird P, Richardson SM, Hoyland JA. 2016. Acidic pH promotes intervertebral disc degeneration: Acid-sensing ion channel -3 as a potential therapeutic target. *Sci Rep* **6**:1–12. doi:10.1038/srep37360

Gorth DJ, Shapiro IM, Risbud M V. 2015. Disc-overy of the Drivers of Inflammation Induced Chronic Low Back Pain: From Bacteria to Diabetes. *Discov Med* **20**:177–184. doi:10.1016/j.physbeh.2017.03.040

Hangai M, Kaneoka K, Hinotsu S, Shimizu K, Okubo Y, Miyakawa S, Mukai N, Sakane M, Ochiai N. 2009. Lumbar intervertebral disk degeneration in athletes. *Am J Sports Med* **37**:149–155. doi:10.1177/0363546508323252

Johnson ZI, Schoepflin ZR, Choi H, Shapiro IM, Risbud M V. 2015. Disc in flames: Roles of TNF-α and IL-1β in intervertebral disc degeneration. *Eur Cells Mater* **30**:104–117. doi:10.22203/eCM.v030a08

Kasra M, Merryman WD, Loveless KN, Goel VK, Martin JD, Buckwalter JA. 2006. Frequency Response of Pig Intervertebral Disc Cells Subjected to Dynamic Hydrostatic Pressure. *Wiley Intersci* 1967–1973. doi:10.1002/jor

Kerr GJ, Veras MA, Kim MKM, S?guin CA. 2017. Decoding the intervertebral disc: Unravelling the complexities of cell phenotypes and pathways associated with degeneration and mechanotransduction. *Semin Cell Dev Biol* **62**:94–103. doi:10.1016/j.semcdb.2016.05.008

Khurana S, Schivo S, Plass JRM, Mersinis N, Scholma J, Kerkhofs J, Zhong L, van de Pol J, Langerak R, Geris L, Karperien M, Post JN. 2021. An ECHO of Cartilage: In Silico Prediction of Combinatorial Treatments to Switch Between Transient and Permanent Cartilage Phenotypes With Ex Vivo Validation. *Front Bioeng Biotechnol* **9**. doi:10.3389/fbioe.2021.732917

Koy T, Zange J, Rittweger J, Pohle-Fröhlich R, Hackenbroch M, Eysel P, Ganse B. 2014. Assessment of lumbar intervertebral disc glycosaminoglycan content by gadolinium-enhanced MRI before and after 21-days of head-down-tilt bedrest. *PLoS One* **9**:e112104. doi:10.1371/journal.pone.0112104

Krumsiek J, Pölsterl S, Wittmann DM, Theis FJ. 2010. Odefy - From discrete to continuous models. *BMC Bioinformatics* **11**:233. doi:10.1186/1471-2105-11-233

Le Maitre CL, Freemont AJ, Hoyland JA. 2005. The role of interleukin-1 in the pathogenesis of human intervertebral disc degeneration. *Arthritis Res Ther* **7**:R732–R745. doi:10.1186/ar1732

Le Maitre CL, Hoyland JA, Freemont AJ. 2007. Catabolic cytokine expression in degenerate and herniated human intervertebral discs: IL-1beta and TNFalpha expression profile. *Arthritis Res Ther* **9**:R77. doi:10.1186/ar2275

Luoma K, Riihimäki H, Luukkonen R, Raininko R, Viikari-Juntura E, Lamminen A. 2000. Low Back Pain in Relation to Lumbar Disc Degeneration. *Spine (Phila Pa 1976)* **25**:487–492. doi:10.1002/ca.22404

MacLean JJ, Lee CR, Alini M, Iatridis JC. 2005. The effects of short-term load duration on anabolic and catabolic gene expression in the rat tail intervertebral disc. *J Orthop Res* **23**:1120–1127. doi:10.1016/j.orthres.2005.01.020

MacLean JJ, Lee CR, Alini M, Iatridis JC. 2004. Anabolic and catabolic mRNA levels of the intervertebral disc vary ... *J Orthop Res* **22**:1193–1200. doi:10.1016/.j.orthres.2004.04.004

Maroudas A, Stockwell RA, Nachemson A, Urban J. 1975. Factors involved in the nutrition of the human lumbar intervertebral disc: cellularity and diffusion of glucose in vitro. *J Anat (J Anat)* **120**:113–130.

Medzhitov R. 2008. Origin and physiological roles of inflammation. *Nature* **454**:428–435. doi:10.1038/nature07201

Mendoza L, Xenarios I. 2006. A method for the generation of standardized qualitative dynamical systems of regulatory networks. *Theor Biol Med Model (Theor Biol Med Model* **3**:13. doi:10.1186/1742-4682-3-13

Mitchell UH, Bowden JA, Larson RE, Belavy DL, Owen PJ. 2020. Long-term running

in middle-aged men and intervertebral disc health , a cross-sectional pilot study. *PLoS One* **15**:e0229457. doi:10.1371/journal.pone.0229457

Mitsos A, Melas IN, Morris MK, Saez-Rodriguez J, Lauffenburger DA, Alexopoulos LG. 2012. Non Linear Programming (NLP) Formulation for Quantitative Modeling of Protein Signal Transduction Pathways. *PLoS One* **7**. doi:10.1371/journal.pone.0050085

Molinos M, Almeida CR, Caldeira J, Cunha C, Goncalves RM, Barbosa MA. 2015. Inflammation in intervertebral disc degeneration and regeneration. *J R Soc Interface* **12**:20141191. doi:10.1098/rsif.2014.1191

Morris MK, Saez-Rodriguez J, Sorger PK, Lauffenburger DA. 2010. Logic-Based Models for the Analysis of Cell Signaling Networks. *Biochemistry* **49**:3216–3224. doi:10.1021/bi902202q

Nachemson A. 1969. Intradiscal measurements of ph in patients with lumbar rhizopathies. *Acta Orthop Scand (Acta Orthop Scand)* **40**:23–42. doi:10.3109/17453676908989482

Nachemson A, Elfström G. 1970. Intravital dynamic pressure measurements in lumbar discs. *Scand J Rehabil Medicat*.

NASA. 2011. Astronauts answer student questions.

Neidlinger-Wilke C, Mietsch A, Rinkler C, Wilke HJ, Ignatius A, Urban J. 2012. Interactions of environmental conditions and mechanical loads have influence on matrix turnover by nucleus pulposus cells. *J Orthop Res (J Orthop Res)* **30**:112–121. doi:10.1002/jor.21481

Orton RJ, Sturm OE, Vyshemirsky V, Calder M, Gilbert DR, Kolch W. 2005. Computational modelling of the receptor-tyrosine-kinase-activated MAPK pathway. *Biochem J* **392**:249–261. doi:10.1042/BJ20050908

Pachi A, Ji T. 2005. Frequency and velocity of people walking. *Struct Eng* 36–40.

Purmessur D, Walter B a, Roughley PJ, Laudier DM, Hecht a C, Iatridis J. 2013. A role for TNFα in intervertebral disc degeneration: a non-recoverable catabolic shift. *Biochem Biophys Res Commun* **433**:151–6. doi:10.1016/j.bbrc.2013.02.034

Rinkler C, Heuer F, Pedro MT, Mauer UM, Ignatius A, Neidlinger-Wilke C. 2010. Influence of low glucose supply on the regulation of gene expression by nucleus pulposus cells and their responsiveness to mechanical loading. *J Neurosurg Spine J Neurosurg Spine* **13**:535–542. doi:10.3171/2010.4.SPINE09713

Ruiz Wills C, Foata B, González Ballester MÁ, Karppinen J, Noailly J. 2018. Theoretical Explorations Generate New Hypotheses About the Role of the Cartilage Endplate in Early Intervertebral Disk Degeneration. *Front Physiol* **9**:1–12. doi:10.3389/fphys.2018.01210

Saggese T, Thambyah A, Wade K, McGlashan SR. 2018. Differential Response of Bovine Mature Nucleus Pulposus and Notochordal Cells to Hydrostatic Pressure and Glucose Restriction. *Cartilage* **0**:1–13. doi:10.1177/1947603518775795

Segarra-Queralt M, Neidlin M, Tio L, Monfort J, Monllau JC, González Ballester MÁ, Alexopoulos LG, Piella G, Noailly J. 2022. Regulatory network-based model to

simulate the biochemical regulation of chondrocytes in healthy and osteoarthritic environments. *Sci Rep* **12**. doi:10.1038/s41598-022-07776-2

Sivan SS, Tsitron E, Wachtel E, Roughley PJ, Sakkee N, Van Der Ham F, DeGroot J, Roberts S, Maroudas A. 2006. Aggrecan turnover in human intervertebral disc as determined by the racemization of aspartic acid. *J Biol Chem* **281**:13009–13014. doi:10.1074/jbc.M600296200

Sivan SS, Wachtel E, Tsitron E, Sakkee N, Van Der Ham F, DeGroot J, Roberts S, Maroudas A. 2008. Collagen turnover in normal and degenerate human intervertebral discs as determined by the racemization of aspartic acid. *J Biol Chem* **283**:8796–8801. doi:10.1074/jbc.M709885200

Stokes IAF, Iatridis JC. 2004. Mechanical conditions that accelerate intervertebral disc degeneration: Overload versus immobilization. *Spine (Phila Pa 1976)* **29**:2724–2732. doi:10.1097/01.brs.0000146049.52152.da

Takatalo J, Karppinen J, Näyhä S, Taimela S, Niinimäki J, Blanco Sequeiros R, Tammelin T, Auvinen J, Tervonen O. 2017. Association between adolescent sport activities and lumbar disk degeneration among young adults. *Scand J Med Sci Sport* **27**:1993–2001. doi:10.1111/sms.12840

Vernillo G, Giandolini M, Edwards WB, Morin JB, Samozino P, Horvais N, Millet GY. 2017. Biomechanics and Physiology of Uphill and Downhill Running. *Sport Med* **47**:615–629. doi:10.1007/s40279-016-0605-y

Videman T, Sarna S, Battié MC, Koskinen S, Gill K, Paananen H, Gibbons L. 1995. The Long-Term Effects of Physical Loading and Exercise Lifestyles on Back-Related Symptoms, Disability, and Spinal Pathology Among Men. *Spine (Phila Pa 1976)* **20**:699–709. doi:10.1097/00007632-199503150-00011

Walsh AJL, Lotz JC. 2004. Biological response of the intervertebral disc to dynamic loading. *J Biomech* **37**:329–337. doi:10.1016/S0021-9290(03)00290-2

Walter B, Korecki C, Purmessur D, Roughley P, Michalek A, Iatridis J. 2012. Complex Loading Affects Intervertebral Disc Mechanics and Biology. *Osteoarthr Cartil* **19**:1011–1018. doi:10.1016/j.joca.2011.04.005.

Wilensky U. 1999. NetLogo.

Wilke HJ, Neef P, Caimi M, Hoogland T, Claes LE. 1999. New in vivo measurements of pressures in the intervertebral disc in daily life. *Spine (Phila Pa 1976)* **24**:755–62. doi:10.1097/00007632-199904150-00005

Yue H, Brown M, Knowles J, Wang H, Broomhead DS, Kell DB. 2006. Insights into the behaviour of systems biology models from dynamic sensitivity and identifiability analysis: a case study of an NF-κB signalling pathway. *Mol BioSyst* **2**:640–649. doi:10.1039/B609442B

Appendix 1

Discussion of the relevance of the obtained results for the NP tissue

This approach aims to contribute to a better understanding of the activity of intervertebral disc (IVD) Nucleus Pulposus (NP) cells by modeling dose- and time-dependent cell regulatory processes that are extremely difficult to measure directly either *in vitro* or *in vivo*. It uniquely combines experimental data and knowledge with mathematical approaches to estimate cell responses to multifactorial stimulations in micro-environments that include cell nutrition, biochemical and mechanical cues, as it happens *in vivo*. In particular, this is the first *in silico* approach, to our knowledge, that allows to approximate combined effects of mag and freq in intricate dose- and time dependent loading conditions on cell activity (CA). Results are subsequently analyzed in context of the NP.

Predictions of daily moving habits (Figure 6). Fluctuating mechanical stimuli affect the CA in terms of both tissue proteins and protease mRNA expression. Thereby, the cell response to different stimulus concentrations does not seem to follow a systematic pattern, especially for the motions expected to involve catabolic CA. For example, while two-hours sitting with a round back and hiking with extra weight were predicted to particularly upregulate the mRNA expressions of Col-I, followed by ADAMTS4, jogging and vibration might rather trigger MMP3 mRNA expressions (Figure 6, B1).

Moving habits that were generally less related with IVD degeneration were sitting (office workers) (Luoma et al., 2000) and walking (Belavý et al., 2017; Takatalo et al., 2017) . In contrast, moving habits classically related to IVD degeneration or to catabolic changes in NP cell responses were weight lifting (Videman et al., 1995), heavy work (carpenters) (Luoma et al., 2000) or whole body vibration exposure (machine drivers) (Luoma et al., 2000). Model simulations are in agreement with such findings, as they predict walking and hiking without

extra weight to be highly anabolic, followed by sleeping and sitting with active back (Figure 6, B1, B2-B5). Accordingly, walking with extra weight or vibrations were predicted by the model to cause a quite catabolic cell response (Figure 6, B1, B6 & B9). However, hiking does not seem to be specifically linked to IVD degeneration, which could be explained with the use of supporting hip belts for (heavy) backpacks. Hence, hikers most probably carry heavy weights rather on their hips than on their shoulders and CA profiles of hikers generally rather resemble the predictions seen for "hiking without extra weight" (Figure 6, B1, B5). Interestingly, sitting with a round back was also catabolic in contrast to sitting with an active back (Figure 6, B3 vs. B8), which nicely corresponds to current ergonomic paradigms.

A possible limitation related with the modelling of the effect of mag and freq is that rodent experimental data had to be used to estimate the weighting factors and time dependencies of different CA. Moreover, there is also a lack of further individualization of time-sensitivities and adjustment factors between mag and freq, due to the limited availability of experimental data for quantification. Likewise, more experimental evidence about the relationship between proinflammatory cytokines and (physiological) loading parameters would contribute to confirm or adapt current modelling assumptions. Eventually, to determine weighting factors, ideally, the maximal effect of a stimulus within a physiological range on a CA should be addressed in experimental studies to be fully exploited in the model. For example, the available data about the mechanostimulation were measured at 1 MPa and 0.01 Hz, 0.2 Hz and 1 Hz, respectively (MacLean et al., 2004). *In vivo* measurements in humans clearly indicate that the physiological range is much broader (Nachemson and Elfström, 1970; Wilke et al., 1999). Consequently, our weighting factor for mag and freq might have been underestimated compared to the effect of nutrient environments, for which measurements over the whole physiological range were available.

Whilst IVD aging appears to be a physiological adaptation of the tissue, accelerated IVD degeneration is not affecting everyone, despite the catabolic shifts possibly caused by moving habits that many people experience more or less frequently (e.g. carrying heavy weights on the shoulders, exposure to vibration). Assuming that acute physiological moving habits are well regulated by the human organism, stimulus chronicity and, therefore, the factor time, seems to be important in IVD degeneration. Furthermore, the high diversity of cellular responses due to different combinations of stimuli suggests that the mechanisms finally leading to (micro-) injuries are manifold, without following one general systematic pattern, which would go along with the high variability of phenotypes in IVD degeneration.

The impact of chronicity is particularly interesting in the model predictions for jogging. The anabolism of jogging has a strongly time dependent component. Whilst its accumulated PN-activity was predicted to be considerably lower than e.g. walking (Figure 6, B1), insights into the evolution over time (Figure 6, B7) suggest that the catabolic impact is pronounced after two hours of jogging, whilst jogging for one hour is still largely anabolic. Accordingly, findings in literature regarding the effect of jogging are controversial: whereas a study of young adults found relationship between frequent jogging and degenerative changes in lumbar IVD (Takatalo et al., 2017), other findings did not reveal a significant effect (Hangai et al., 2009) or jogging was found to be beneficial compared to a non-physiologically active control group (Belavý et al., 2017; Mitchell et al., 2020). Assuming that the chronicity of cell stressors is crucial in the dynamics of IVD degeneration, as suggested by the model predictions, a frequent switch among different moving habits can contribute to reduce the risk of IVD degeneration and/or decelerate its development.

Predictions of the effect of microgravity and daily life under gravity and for different proinflammatory cell states (CS). Simulations of a daily life on earth show low to minimal

Col-I and protease mRNA expressions and elevated Agg and Col-II mRNA expressions. Due to the presence of proinflammatory cytokines, protease mRNA expressions rise, whilst the mRNA expressions of tissue proteins show an overall slight decrease (Appendix 1 – figure 1, A2, A3). Exposure to microgravity over six months led to a general downregulation of the expression of tissue proteins by predicting a roughly 25% and 20% lower PN-activity of Agg and Col-II mRNA expression, respectively, independently of the CS (Appendix 1 – figure 1, A1, left vs. A2). MMP3 mRNA expression was not particularly affected by simulations of microgravity. In contrast, ADAMTS4 mRNA expression was predicted to slightly rise, which could be generally attributed to the end of the stay in space (Appendix 1 – figure 1, A1, right). Independently of the simulated condition, Col-II mRNA expression is lower, relative to Agg mRNA expression (Appendix 1 – figure 1).

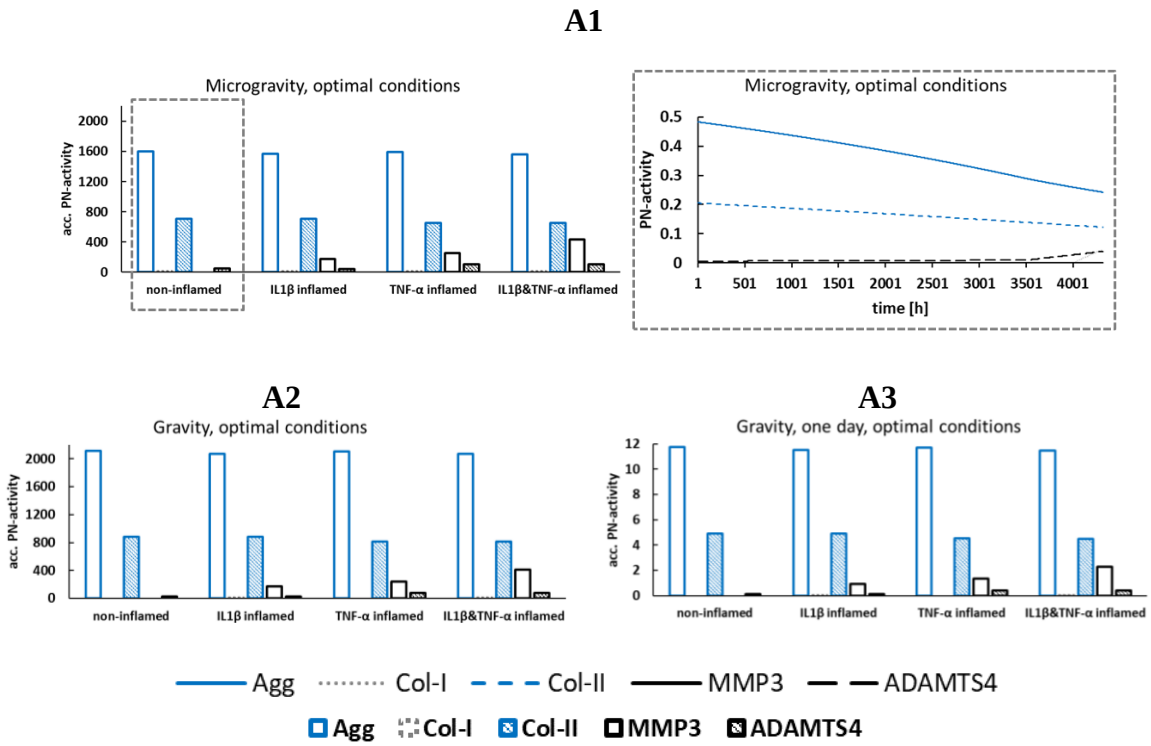

Appendix 1 – figure 1: estimated CA profiles after six months of exposure to microgravity (A1, left), for an average daily moving habit (A3) and its accumulation over six months (A2). The effect of exposure to microgravity is additionally shown for non-inflamed cells as a continuous development over time (A1, right). Non-degenerated nutritional conditions were used (5 mM glucose, pH 7.1). Please note that the graphs A1 and A2 were provided in Figure 5, and were hereby repeated for the context of graph A3.

Model predictions simulating daily life under gravity (Appendix 1 – figure 1, A2) were in agreement with general expectations: minimal or close to minimal CA for MMP3 and ADAMTS4 mRNA expressions go along with low MMP3 and ADAMTS4 protease levels found within the tissue (Molinos et al., 2015). Elevated CA for Agg and Col-II mRNA expressions reflect the cellular function to maintain the tissue. Generally, lower CA for Col-II than for Agg along with both, a lower tissue turnover of collagen compared to Agg (Sivan et al., 2008, 2006) and a lower fraction of Col-II tissue compared to Agg (Baumgartner et al., 2021). The predicted catabolic shift in TNF-α inflamed cells is in agreement with experimental findings that identify TNF-α as a strong catabolic mediator (Purmessur et al., 2013). IL1β was

predicted to be less catabolic than TNF-α, which coincides with its possible role in normal cell homeostasis (Le Maitre et al., 2007).

Compared to gravity, simulated exposure to microgravity usually caused a downregulation of glycosaminoglycan contents (Appendix 1 – figure 1, A1 vs. A2), which is supported by various animal models (Belavy et al., 2016). Agg is the major proteoglycan in cartilaginous tissues. It is a complex macromolecule with numerous chondroitin sulfate glycosaminoglycan chains. Because these chains are negatively charged, Agg are responsible to attract water through Donnan osmosis effects. A reduced Agg content goes along with a reduced fixed charge density, which in turn could be related to a lower hydration of the IVD (Baumgartner et al., 2021). Although such findings at first glance would explain disc desiccations found after long-term space flights (Garcia et al., 2018), the slow turnover of tissue proteins with half-lives of around 12 (Agg) and 95 (collagen) years (Sivan et al., 2008, 2006), questions whether the effect of tissue protein downregulation becomes visible *in vivo* at the tissue level, after only six months.

The model predicts ADAMTS4 to substantially rise within the last weeks of the research stay, i.e. after around 3500 h (Appendix 1 – figure 1, A1, right). The value of the adjustment factor is deterministic for the velocity of the continuous evolution of CA profiles over time. Given that the adjustment factor could not be specified yet between mag and freq, and that rather the range, than its effective size was determined (see Methods), a generally prudent interpretation of the specific timepoints observed in continuous CA-profiles is required.

Remarkably, though, the continuous evolution of a CA over time (Appendix 1 – figure 1, A1, right) shows a general trend of a constant low level of proteases within the first months of simulated exposure to microgravity. Such expressions were similar to one simulated day under gravity (Appendix 1 – figure 1, A3). The daily moving habit was chosen to be quite “optimal”, while “suboptimal” moving under gravity (i.e. carrying heavy weights or exposure to vibration)

was responsible for the upregulation of protease activity (Figure 6, B6-B9). Under microgravity such “suboptimal” stimuli cannot be represented; consequently the protease mRNA expression was kept low, which might contribute to an increased swelling behavior of the IVD along time. Swelling behavior of the IVD was particularly observed under head-down-tilt bedrest (Koy et al., 2014), the most common analogue to investigate effects of microgravity. Yet, the existence of IVD swelling during spaceflight is debated, since studies found that pre-to post-flight differences in disc water content after six months exposure to microgravity were either non-significant (Bailey et al., 2018) or, moreover, signs for disc desiccation were observed already during exposure to microgravity in ultrasound images (Garcia et al., 2018).

Hence, the model predicts indications for both, disc desiccation on the one hand, due to a downregulation of tissue protein mRNA expression, whilst, on the other hand, constantly low levels of protease mRNA expression might contribute to findings of disc swelling. Both is actually observed under similar mechanical conditions, i.e. under exposure to microgravity and in bed rest studies. A better understanding of a final consolidation at the tissue level might be obtained by a quantification actual mRNA expressions coupled to a CA. Moreover, besides the mechanical loading conditions, peculiarities of microgravitational conditions, e.g. lumbar spine flattening and possible changes in intradiscal nutrient supply should be considered in future work to confirm or adapt current predictions under microgravity.

Conclusions of the tissue-specific findings

This work is the first contribution that allows to describe relative cell responses within complex, heterogeneous stimulus environments. The aim was to approximate cell responses to a native stimulus environment by considering crucial external and local stimuli. Thanks to the integration of time-dependent effects, this work uniquely allowed to estimate adaptations of

cells to persisting mechanical load patterns over time, as found in daily activities or under exposure to microgravity.

Findings were in good agreement with literature and coincide with observed organ and tissue macroscopic adaptations. Hence, simulations with the PN_t-Methodology indicate that IVD NP degeneration is most probably not the result of one, principal biological response, but it highly depends on the (micro-) environmental stimulus combinations. Results further suggest that chronicity of mechanical loads is key relevant in IVD NP degeneration. Hence, a frequent change of moving habits, e.g. sitting positions, might be beneficial to maintain IVD integrity.

Future work should tackle further detail regarding the effects of exposure to microgravity and it should focus on a more sensitive integration of loading conditions. Eventually, an integration of this approach into (bottom-up or top-down) multiscale approaches is deemed to be key relevant to tackle injury dynamics within the IVD.

Appendix 2

Additional simulations: modelling nutritional conditions as found in early degenerated IVD and predictions of the PN_t-Methodology coupled to a 3D Agent-based model, simulating a multicellular environment

Methods: To simulate most critical impacts of nutritional conditions as expected in early degenerated IVD, the region was chosen where the most adverse nutrient environment was found. Its location and local nutrient concentrations were determined by our in-house mechanotransport finite element (FE) model (Ruiz Wills et al., 2018); the cartilage endplate permeability was adapted as expected at early stages of IVD degeneration and nutrient concentrations were estimated throughout the IVD. Most critical nutrient concentrations were found within the anterior NP around the mid-transverse plane, with a prediction of an average glucose concentration of 0.8901 mM and pH 6.9349.

The PN_t-Methodology was embedded in a 3D Agent-based (AB) model (Netlogo (Wilensky, 1999)) that simulated a NP environment consisting of 4000 agents (diameter 10µm) and a volume of $1mm^3$. Agents represent NP cells at an average density (Maroudas et al., 1975). Agents were randomly placed into the volume and immobile throughout simulations. Each NP cell obtained one out of four cell states; immunonegative or immunopositive for IL1β, for TNF-α or for both IL1β&TNF-α. The setup of the multicellular environment is explained in detail in our previous publication (Baumgartner et al., 2021). In short: the model predicts a global, normalized amount of IL1β and TNF-α mRNA expression according to external stimulus concentrations, based on which the percentage of immunopositive cells for IL1β and TNF-α was determined. Corresponding numbers of inflamed cells were distributed in randomly placed cell clusters. Within regions where IL1β and TNF-α immunopositive cell clusters overlap, cells

were considered to be immunopositive for both, IL1β&TNF-α. The minimal calculation time step was set to 1h.

Results: Early degenerated conditions led to similar CA profiles for non-inflamed and IL1β inflamed cells as found for non-degenerated conditions, but caused a worse catabolic shift under TNF-α presence, under both, gravity and exposure to microgravity. The catabolic shift in cells exposed to TNF-α consists of a downregulation of Col-II and an upregulation of MMP3 and ADAMTS4. In contrast, Agg mRNA expression is similar for non-degenerated and early degenerated conditions, independently from the CS (Appendix 1 – figure 1 vs. Appendix 2 – figure 1).

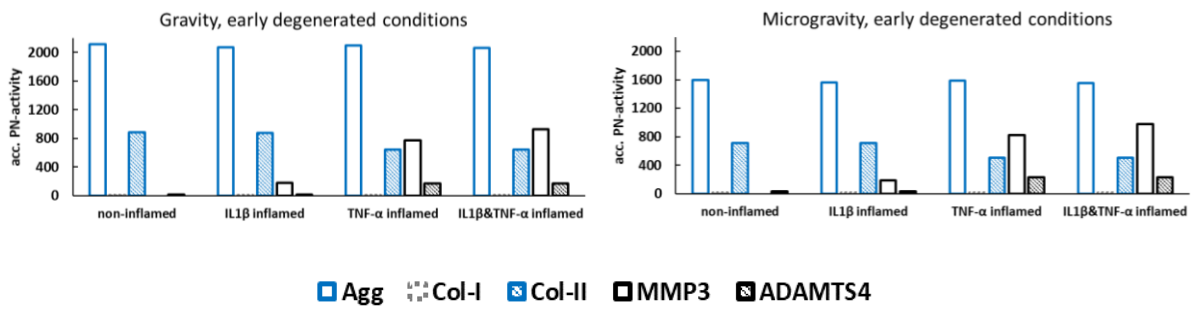

Appendix 2 – figure 1: estimated CA profiles for an average daily moving habit over six months compared to exposure to microgravity for the same period of time. Simulation of an early degenerated nutrient environment.

The percentage of cells immunopositive for IL1β is maintained around 15-16% for all simulated conditions, whilst TNF-α proinflammatory environments rise from around 10-11% for non-degenerated to 15-16% under early degenerated conditions (Appendix 2 – table 1).

Appendix 2 – table 1: predicted, proinflammatory environments within the AB-model for non-degenerated and early degenerated conditions at gravity and under exposure to microgravity. Cells inflamed for both, IL1β&TNF-α were added to the respective percentages of both, TNF-α and IL1β (see Baumgartner et al., 2021). Percentages of inflamed cells are rounded and based on three model runs for each condition.

		IL1β	TNF-α
Non-degenerated	Gravity	~15.5%	~10.5%
	Microgravity	~15.5%	~10.5%
Early degenerated	Gravity	~16%	~15.5%
	Microgravity	~16%	~16%

Discussion: the effect of early degeneration on tissue proteins is small (with the exception of Col-II downregulation under TNF-α presence), which is in agreement with the generally slow development of this disease. However, the change in nutrient concentrations caused an elevated TNF-α presence, leading to a catabolic shift of CA of cells exposed to TNF-α and to an elevated percentage of cells inflamed with TNF-α (Appendix 2 – table 1). Hence, catabolic shifts might be locally enhanced within the NP under early degenerated conditions.

Overall, predicted proinflammatory environments lie within plausible ranges, albeit they still lie within ranges as expected in non-degenerated NP, i.e. 17% $\pm$ 7%, for IL1β and 16% $\pm$ 7%, respectively, for TNF-α (Le Maitre et al., 2007). Hence, the currently estimated percentage of inflamed cells might be conservative and, consequently, as well the catabolic shifts of the CA profiles of inflamed cells are conservative estimations.

Current results might suggest TNF-α inflammation to play a role under early degenerated conditions. However, the prediction of inflammation underlies uncertainties, given that the

effect of loading on proinflammatory cytokine expression is largely unknown. Moreover, critical factors such as effects between proinflammatory cytokines (see Baumgartner et al., 2021) or possible endogenous triggers of inflammation such as ECM breakdown products (Medzhitov, 2008) (i.e. damage-associated molecular patterns) were not considered, which coincides with an overall conservative prediction of inflammation. However, given that model simulations show enhanced protease activity due to the presence of proinflammatory cytokines, (local) accumulation of ECM breakdown products can be presumed. Hence, model results support the hypothesis that an upregulation of proinflammatory environments is initiated by altered protease activities, whilst locally generated ECM breakdown products can secondarily activate the proinflammatory response of NP cells.

Appendix 3

Additional analysis of the performance of the PN_t-Methodology for user-defined conditions around the α-β-threshold

Methods: To investigate the model performance around the α-β-threshold, one loading parameter was set to respective minimal values, i.e. either 0.1 MPa or 0 Hz, whilst the other one was varied, covering the range around the α-β-threshold of the generic functions. Hence, i) a static condition (0 Hz) was simulated under varying loading conditions of 0.90 MPa, 0.95 MPa, 1.00 MPa, 1.05 MPa and 1.10 MPa and ii) dynamic conditions were simulated under a constant load of 0.10 MPa at 2.90 Hz, 2.95 Hz, 3.00 Hz, 3.05 Hz and 3.10 Hz (note that the minimal step increase of loading parameters was set to 0.05). Thereby, the loading conditions 0.90 MPa, 0.95 MPa and 2.90 Hz, 2.95 Hz, 3.00 Hz, respectively, were initally anabolic, whilst higher loading conditions caused catabolic responses (Appendix 3 – figure 1). Optimal nutrient conditions (5 mM glucose, pH 7.1) were simulated and the response of non-inflamed cells was plotted.

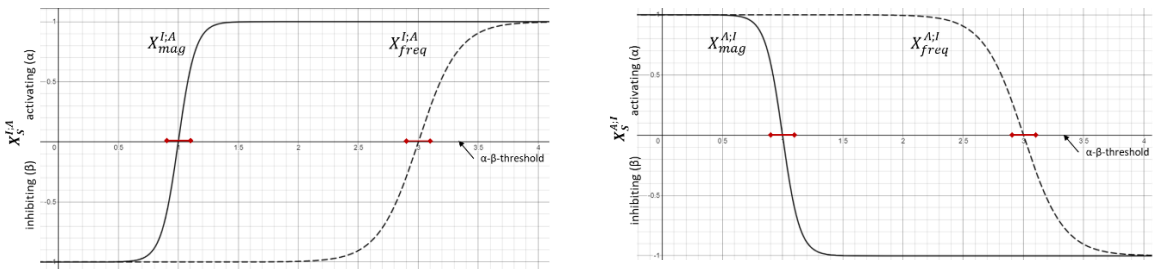

Appendix 3 – figure 1: generic functions reflecting I;A (left) and A;I (right) evolutions, with critical ranges around the α-β-threshold marked as red bars.

Results: Model predictions were influenced by the steepness of the sigmoidal slope and the impact of the respective stimulus on a specific CA. Hence, the steeper the slope, the shorter the time range of incoherent predictions. (Incoherent predictions refer to incorrect results that might

appear due to time-dependent effects within the first hours of calculations. For example, the MMP3 mRNA expressions at 0 Hz and 0.1 MPa; after 2h of persisting loading, the model predicts lowest PN-activity at 1.05 MPa and 3.05 Hz, respectively (Appendix 3 – figure 2).) Moreover, predictions based on the A;I generic function, i.e. tissue protein expressions, quickly converged to the same PN-activity, independently of the initial value of the stimulus (Appendix 3 – figure 2, Agg and Col-II). In contrast, predictions for I;A generic functions (Col-I and protease expressions) converged much slower (Appendix 3 – figure 3). Hence, the PN-activity of I;A generic functions initially converge to two different PN-activities over the first hours of simulation (pronounced in Appendix 3 – figure 2, Col-I, ADAMTS4), depending on their input range (i.e. anabolic or catabolic). Predictions at 1.00 MPa led to systematically erroneous results (Appendix 3 – figure 2, left column).

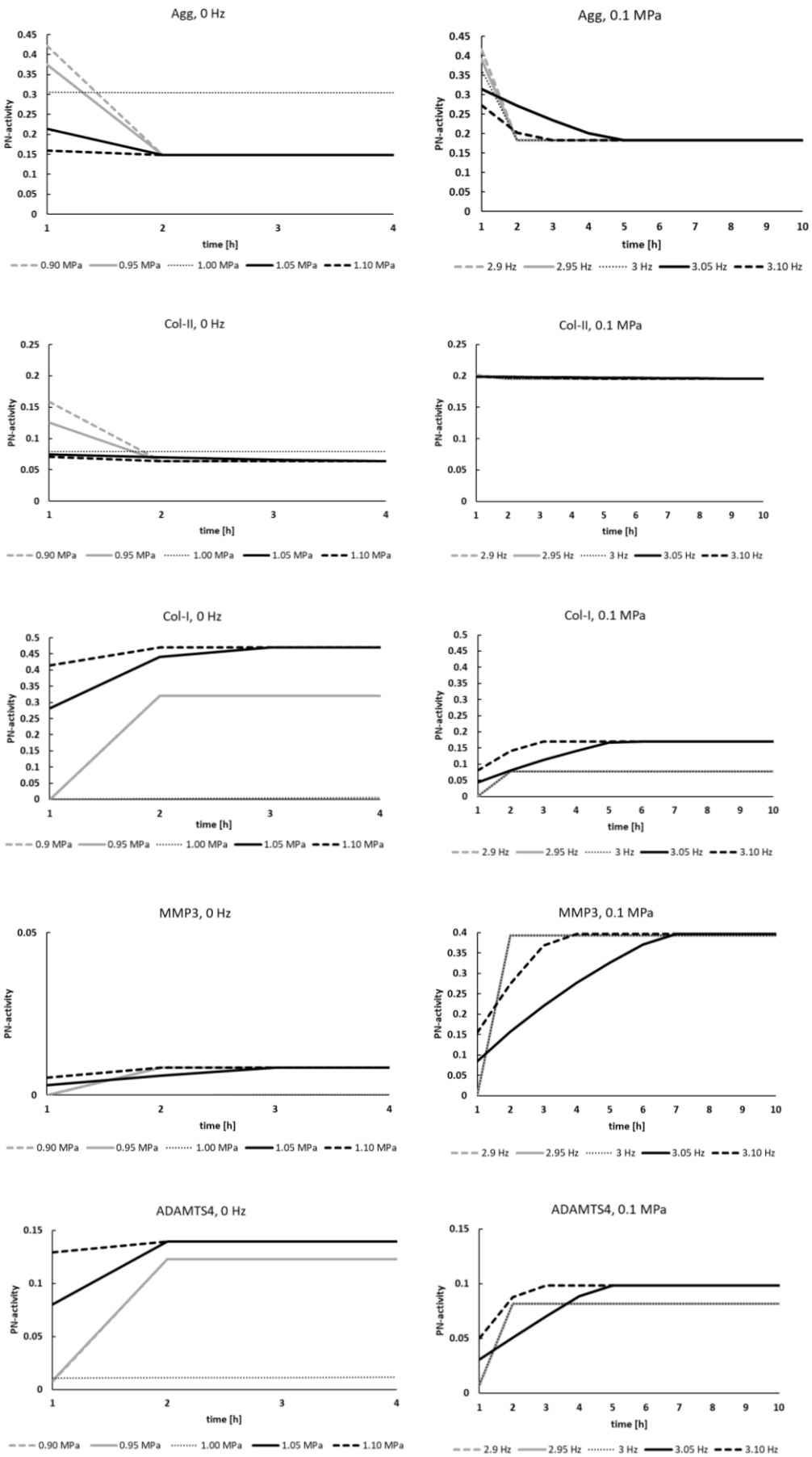
Agg, 0 Hz
PN-activity
time [h]
0.90 MPa
0.95 MPa
1.00 MPa
1.05 MPa
1.10 MPa
Agg, 0.1 MPa
PN-activity
time [h]
2.9 Hz
2.95 Hz
3 Hz
3.05 Hz
3.10 Hz
Col-II, 0 Hz
PN-activity
time [h]
0.90 MPa
0.95 MPa
1.00 MPa
1.05 MPa
1.10 MPa
Col-II, 0.1 MPa
PN-activity
time [h]
2.9 Hz
2.95 Hz
3 Hz
3.05 Hz
3.10 Hz
Col-I, 0 Hz
PN-activity
time [h]
0.9 MPa
0.95 MPa
1.00 MPa
1.05 MPa
1.10 MPa
Col-I, 0.1 MPa
PN-activity
time [h]
2.9 Hz
2.95 Hz
3 Hz
3.05 Hz
3.10 Hz
MMP3, 0 Hz
PN-activity
time [h]
0.90 MPa
0.95 MPa
1.00 MPa
1.05 MPa
1.10 MPa
MMP3, 0.1 MPa
PN-activity
time [h]
2.9 Hz
2.95 Hz
3 Hz
3.05 Hz
3.10 Hz
ADAMTS4, 0 Hz
PN-activity
time [h]
0.90 MPa
0.95 MPa
1.00 MPa
1.05 MPa
1.10 MPa
ADAMTS4, 0.1 MPa
PN-activity
time [h]
2.9 Hz
2.95 Hz
3 Hz
3.05 Hz
3.10 Hz

Appendix 3 – figure 2: predictions around the α-β-threshold of the generic functions of mag (left) and freq (right). Note that predictions at 0.9 and 0.95 MPa are identical for Col-I and MMP3 mRNA expressions and almost identical for ADAMTS4 mRNA expression at 0 Hz (left column). Likewise, predictions at 2.90 Hz, 2.95 Hz and 3.00 Hz have the same values for Col-I and MMP3 mRNA expressions and almost identical values in case of ADAMTS4 mRNA expressions at 0.1 MPa (right column).

Discussion: the influence of the steepness of the sigmoidal shape is not surprising, given that the time sensitivity is based on the generic functions. Hence, a less steep slope includes a smaller effect of time in each time step, which leads to a slower evolution of the CA over time. Stimulus doses closest to the α-β-threshold are 1.00 MPa and 3.00 Hz, respectively (Appendix 3 – figure 1). Whilst the prediction of 1.00 MPa generally led to incorrect predictions (Appendix 3 – figure 2, left column), predictions around 3.00 Hz did not show any peculiar behavior (Appendix 3 – figure 2, right column). The reason is that 3.00 Hz is still considered as an anabolic stimulus by the algorithm, whilst 1.00 MPa is already slightly catabolic. Hence, according to the setup of time sensitivity, anabolic stimuli closely to the α-β-threshold rapidly lose their anabolism, whilst the programming of the latency time assumes that weak catabolic stimulus doses are longer tolerated than strong catabolic stimulus doses. This explains why PN-activities after short time periods might generally lead to incoherent results, e.g. the effect of 3.05 MPa on Agg mRNA expression (Appendix 3 – figure 2, “Agg, 0 Hz”) after two hours show a higher PN-activity than any other condition. To overcome such limitations, it is generally recommended to rather approximate the PN activity by an extrapolation of results calculated at higher and lower stimulus doses.

Whilst the effect of time on CA based on A;I generic functions, i.e. Agg and Col-II mRNA expressions, converge to same PN-activities within a short period of time (with exception of the previously addressed predictions at 1.00 MPa), mRNA expression based on I;A generic

functions converge to two different levels of PN-activities, depending on the anabolic or catabolic character of the initial stimulus dose. Thereby, initially anabolic loading led to a generally lower catabolic response than initially catabolic loads (Appendix 3 – figure 2). This difference is caused by the first fraction of the inhibiting term. The weight that this fraction provides to the inhibiting term is different from the weight within the activating portion of the PN-equation. This is considered to be a limitation of the PN-equation. However, qualitatively the results are coherent; initially anabolic values remain more anabolic over time. The effect vanishes as soon as the inhibiting term of the PN-equation becomes 0, which is subsequently demonstrated by plotting the evolution of Col-I and Agg mRNA expressions over time (Appendix 3 – figure 3). Note that the freq was elevated from 0 Hz to 2 Hz, to accelerate the decrease of the inhibiting term of the PN-equation to zero.

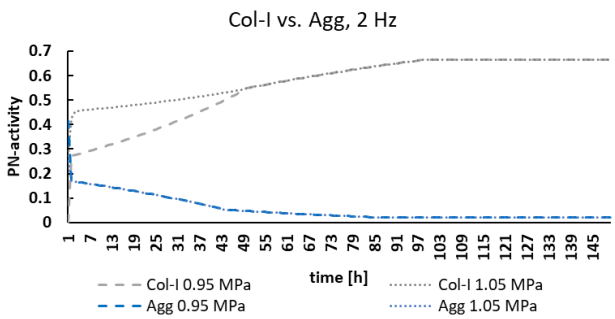

Appendix 3 – figure 3: evolution of initially anabolic (0.95 MPa) and catabolic (1.05 MPa) mag doses over time on the example of Col-I and Agg. The same PN-activity for Col-I is obtained after 50 h of stimulus exposure. In contrast, the PN-activity of Agg exposed to different mag are already reached after 4 h stimulus exposure.

Appendix 4

Overview of weighting factors considered in the system of interest of the NP

The subsequent Appendix 4 – table 1 contains an overview of the weighting factors used to calculate the current results. The information for indirect mechanotransduction was previously presented, together with the mathematical description of weighting factors (Baumgartner et al., 2021). In short: weighting factors were obtained from experimentally found x-fold mRNA expressions (ϵ). ϵ were translated into a "cellular effort" ($f(\epsilon)$), which allows to equalize up- and downregulations of mRNA expressions compared to a control value (Appendix 4 – table 1).

Appendix 4 – table 1: Overview of weighting factors for the tackled system of interest of the NP. Individual weighting factors were derived from the cellular effort ($\boldsymbol{f(\epsilon)}$), based on x-fold mRNA expressions ($\boldsymbol{\epsilon}$). The scaling factor $\boldsymbol{\vartheta_{\theta_{max}}} = \boldsymbol{\vartheta_1 = 28.7}$ was determined by the S-CA relationship pH-MMP3. NS: Not significant; act: activating; inh: inhibiting; *: estimated $\boldsymbol{\epsilon}$; glc: glucose.

Stimulus	**mRNA**	$\boldsymbol{\epsilon}$	$\boldsymbol{f(\epsilon)}$	$\boldsymbol{\theta_S^{CA}}$ ($\vartheta_1 = 28.7$)	**Source**	**Cell type**
Glc	Agg	NS, act	-	0.0100	(Rinkler et al., 2010)	human
	Col-I	NS, act	-	0.0100	(Rinkler et al., 2010)	human
	Col-II	NS, act	-	0.0100	(Rinkler et al., 2010)	human
	MMP3	NS, act	-	0.0100	(Rinkler et al., 2010)	human
	ADAMTS4	NS, act	-	0.0100	(Baumgartner et al., 2021)	bovine

	IL1β	NS, act	-	0.0100	(Baumgartner et al., 2021)	bovine
	TNF-α	NS, act	-	0.0100	(Baumgartner et al., 2021)	bovine
pH	Agg	0.37	2.7027	0.0942	(Gilbert et al., 2016)	human
	Col-I	NS, act	-	0.0100	(Gilbert et al., 2016)	human
	Col-II	0.63	1.5873	0.0553	(Neidlinger-Wilke et al., 2012)	bovine
	MMP3	28.7	28.7000	1.0000	(Gilbert et al., 2016)	human
	ADAMTS4	5.7	5.7000	0.1986	(Gilbert et al., 2016)	human
	IL1β	81	81.0000	2.8223	(Gilbert et al., 2016)	human
	TNF-α	NS, act	-	0.0100	(Gilbert et al., 2016)	human
IL1β	Agg	0.45*	2.2222	0.0774	(Le Maitre et al., 2005)	human
	Col-I	NS, act	-	0.0100	(Le Maitre et al., 2005)	human
	Col-II	NS, inh	-	0.0100	(Le Maitre et al., 2005)	human
	MMP3	10.8*	10.8000	0.3763	(Le Maitre et al., 2005)	human
	ADAMTS4	NS, inh	-	0.0100	(Le Maitre et al., 2005)	human
TNF-α	Agg	NS, inh	-	0.0100	(Baumgartner et al., 2021)	bovine

	Col-I	0.31	3.2258	0.1124	(Baumgartner et al., 2021)	bovine
	Col-II	0.06	16.6667	0.5807	(Baumgartner et al., 2021)	bovine
	MMP3	26.85	26.8500	0.9355	(Baumgartner et al., 2021)	bovine
	ADAMTS4	5.77	5.7700	0.2010	(Baumgartner et al., 2021)	bovine
Mag	Agg	10	10	0.3484	(MacLean et al., 2004)	rat
	Col-I	25	25	0.8711	(MacLean et al., 2004)	rat
	Col-II	4	4	0.1394	(MacLean et al., 2004)	rat
	MMP3	NS	-	0.0100	(MacLean et al., 2004)	rat
	ADAMTS4	4	4	0.1394	(MacLean et al., 2004)	rat
	TNF-α	NS	-	0.0100	Indications(Dudli et al., 2012; Gawri et al., 2014)	
	IL1β	NS	-	0.0100	Indications(Walter et al., 2012)	
Freq	Agg	10 1.05*	$\frac{10}{1.05}$ (= 9.5238)	0.3318	(MacLean et al., 2004)	rat
	Col-I	25 0.50*	$\frac{25}{2}$ (=12.5000)	0.4355	(MacLean et al., 2004)	rat

Col-II	NS	-	0.0100	(MacLean et al., 2004)	rat
MMP3	15 1.02*	$\frac{15}{1.02}$ (=14.7059)	0.5124	(MacLean et al., 2004)	rat
ADAMTS4	8 2.66	$\frac{8}{2.66}$ (=3.0075)	0.1048	(MacLean et al., 2004)	rat
TNF-α	NS	-	0.0100	No information found	
IL1β	NS	-	0.0100	No information found	